Potential Vorticity Inversion for Tropical Cyclones Using the Asymmetric Balance Theory

J. DOMINIQUE MÖLLER AND SARAH C. JONES

Meteorologisches Institut, Universität München, Munich, Germany

(Manuscript received 14 May 1996, in final form 7 May 1997)

ABSTRACT

A three-dimensional model is developed, based upon the recently derived asymmetric balance (AB) formulation of Shapiro and Montgomery, to study the evolution of rapidly rotating vortices, including hurricanes. A particular advantage of the AB theory, unlike other balanced models, is its ability to incorporate divergence of the same order as the vorticity. The main assumption of the AB theory is that the squared local Rossby number $\ll 1$, where the squared local Rossby number is defined by the ratio of the orbital frequency squared to the inertial stability. The AB theory leads to a set of prognostic equations that are manipulated so that the first- and second-order local time tendencies can be evaluated diagnostically at a given time. Using the diagnostic version of the AB equations the potential vorticity (PV) distribution from a primitive equation (PE) model is inverted to obtain the corresponding balanced height and wind fields. As far as the authors are aware, this is the first time that the AB equations have been solved in three dimensions.

A calculation is described in which the PE model is initialized with an axisymmetric barotropic vortex in a vertical shear flow. Vertical shear leads to a wavenumber 1 asymmetry in the PV distribution. Associated with this asymmetry is a component of flow across the vortex center, which has an influence on the vortex motion. In this calculation the PE model provides not only the PV distribution but also the data to test the accuracy of the newly derived AB theory. The wavenumber 1 distributions of the radial, tangential, and vertical velocity fields diagnosed using the AB theory are compared with the results of the PE model. The agreement in amplitude and orientation is found to be good. The relative error between the amplitude maxima of the velocities in the PE calculations and the diagnostically derived AB fields is comparable with the maximum size of the squared local Rossby number. Although the main assumption of the AB theory is not strictly satisfied in these calculations, meaningful comparisons can be made between the PE results and the AB solutions. Presenting the results of the velocity fields in the moving coordinate system and use of the piecewise inversion makes it possible to isolate the influence of the upper-level PV anomaly on the lower-level part of the vortex and the influence of the lower-level PV anomaly on the upper-level part of the vortex.

In a further calculation a vortex is initialized in a horizontal shear flow and diabatic heating and friction are included. The prescribed heating is related to the boundary layer convergence. The heating produces strong vertical gradients in the tangential wind so that the PV of the symmetric vortex becomes negative after 24 h. As in the nonlinear balance equations, the AB formulation requires the PV to be positive in order to be able to find a solution.

A comparison between the velocity fields of the PE model and the diagnostically derived AB solutions after 12 h shows a good agreement in amplitude and orientation at lower levels but significant differences in amplitude at upper levels. At upper levels a vortex has not developed after 12 h and the standard Rossby number is the appropriate measure of the validity and accuracy as in the quasigeostrophic approximation. As in the case with no heating the agreement between the velocity components of the AB and PE model depends on the magnitude of the squared local Rossby number or standard Rossby number.

1. Introduction

The dynamics of atmospheric flows can be studied using primitive equation (PE) models with full physics or using filtered models, such as balanced models, for understanding the Hadley circulation (Schubert et al. 1991) or midlatitude cyclogenesis (Davis and Emanuel 1991; Montgomery and Farrell 1992). Balanced models, including those based on the standard balance equations (Charney 1962) or those based on the geostrophic momentum approximation (Hoskins 1975), are filtered systems, whose accuracy lies between the primitive and the quasigeostrophic equations. For this reason they are sometimes called ''intermediate models'' (McWilliams and Gent 1980). Because the balanced models exclude phenomena such as gravity waves, which are often unimportant for understanding the large-scale flow, they provide for a simplified description of the evolution of weather systems. A fundamental quantity for atmospheric flows is the potential vorticity (PV), which is materially conserved in the absence of diabatic and frictional processes. In a balanced system one can use PV to diagnose the complete structure of the flow. The basis of this diagnosis is called the ''in-

Corresponding author address: Dr. J. D. Möller, Department of Atmospheric Science, Colorado State University, Fort Collins, CO 80523-1371.
E-mail: jdm@fjortoft.atmos.colostate.edu

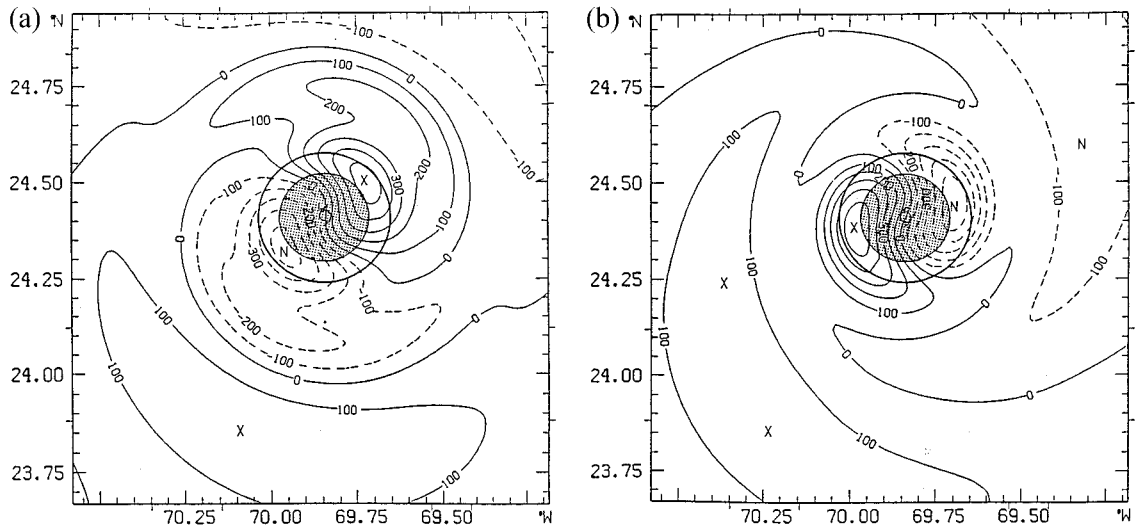

FIG. 1. Wavenumber-1 component of (a) the relative vorticity and (b) the horizontal divergence of Hurricane Gloria at a height of 700 hPa. Maximum value of (a) and (b) about 500×10^{-6} s^{-1}.

vertibility principle,'' which states that with a known PV distribution, a prescribed balance condition, a prescribed reference state, and with appropriate boundary conditions, it is possible to determine the complete mass and velocity fields of that balanced state (Hoskins et al. 1985).

Much of our understanding of the dynamics of tropical cyclone motion is based on results from barotropic vortex models in which the wavenumber-1 asymmetry of the relative vorticity distribution has been shown to play an important role (Fiorino and Elsberry 1989; Shapiro and Ooyama 1990; Smith et al. 1990). In the barotropic framework the vorticity asymmetries can be inverted to obtain the streamfunction asymmetries, from which the velocity of the flow across the vortex center can be determined; this velocity is to a close approximation the translation velocity of the vortex (Smith et al. 1990). A natural extension of the ideas to baroclinic vortices would point to the importance of the wavenumber-1 asymmetry in the PV distribution. With the aid of a balanced model appropriate for tropical cyclones the PV asymmetries can be inverted also to obtain the flow across the vortex axis.

Tropical cyclones are weather systems with strong upward motion, which implies that the horizontal divergence and vertical advection may be large. In addition, there is strong curvature in tropical cyclones. The presence of both strong curvature and strong divergence means that many balance conditions are not formally valid. One exception is the asymmetric balance (AB) formulation of Shapiro and Montgomery (1993, henceforth referred to as SM), which was derived recently to study the evolution of rapidly rotating vortices, including tropical cyclones. The AB formulation takes into account the full dynamics of the vortex core region and represents the outer region or far field as a quasigeostrophic flow. The theory uses the fact that in the near field all vortex asymmetries are weak compared with the symmetric (wavenumber 0) circulation and it assumes that the wavenumber-1 component dominates the total asymmetry. Shapiro and Montgomery justify these assumptions using data from Hurricane Gloria. The major advantage of the AB theory is that, in principle, there is no restriction on the magnitude of the horizontal divergence and the vertical advection. Therefore, the theory may be at least as accurate for tropical cyclones as nonlinear balanced models, if not more so under certain circumstances. For example, in the core region of a hurricane, where divergence can be large, one could imagine that the AB theory would give more accurate results than the nonlinear balance models, as the latter formally neglect the divergent part of the wind fields.

A nested analysis of dropwindsonde and Doppler radar data for Hurricane Gloria confirms that the asymmetric divergence has a similar magnitude to the asymmetric vorticity (M. Montgomery and J. Franklin 1995, personal communication). As an example, Fig. 1 shows the azimuthal wavenumber-1 contribution of the relative vorticity and divergence of Hurricane Gloria at a height of 700 hPa. The shaded circle in the center of the hurricane shows the area where no data were available and the solid thick circle defines the radius of maximum wind. The wavenumber-1 distribution of the vorticity (with a maximum of 500×10^{-6} s^{-1}) is about one order smaller in magnitude than that of the total vorticity field. The magnitude of the wavenumber-1 divergence, however, is nearly the same as that of the total divergence field and has the same size as the wavenumber-1 vorticity. The reason lies in the highly asymmetric divergence structure associated with a convective band near Gloria's center (Franklin et al. 1993, Fig. 12).

The AB theory leads to a set of prognostic equations that, in principle, may be integrated forward in time. How-

ever, their complexity compared with the primitive equations, and that they are no more than an approximation to the latter, raises the question of the advisability of trying to solve them in time. Nevertheless, the equations may be manipulated so that the first- and second-order local time tendencies can be evaluated diagnostically at a given time. The PV provided by model output or real data can be inverted at a given time to obtain the corresponding balanced height and wind fields. It is the latter approach that is followed in the present paper, where we use a PE model to calculate the evolution of a vortex and the AB theory to diagnose and interpret the results. In this way one has the advantage of the accuracy of the primitive equations plus the simplified representation of the dynamics offered by the approximate theory. An additional advantage is that when using the AB theory diagnostically it is not necessary to predict the translation velocity and acceleration of the moving coordinate system in which the AB theory is formulated. Although the main assumption of the AB theory, that the squared local Rossby number is very small, is not strictly satisfied in these calculations, meaningful comparisons can be made between the PE results and the AB solutions. For diagnostic purposes, which we utilize here, it is quite reasonable to obtain qualitatively correct answers even if they are not quantitatively accurate. In a prognostic calculation, on the other hand, the quantitative accuracy could be very important as any errors may accumulate in time.

The AB theory assumes that the structure of the symmetric vortex is known and uses the symmetric quantities to calculate the balanced wind and mass fields of the perturbations. As discussed above, the wavenumber-1 asymmetry should be the dominant asymmetry in the vortex core. The three-dimensional AB model is applied to different situations in which a vortex is embedded in a horizontal or vertical shear flow. Calculations are carried out with or without representations of cumulus heating and surface friction. The results presented here provide insight into the influence of heating and friction on both the PV distribution and the corresponding velocity fields of a tropical cyclone. They provide also a basis for applying ''PV thinking'' to real data cases, complementing the recent studies of Molinari et al. (1995), Shapiro and Franklin (1995), and Wu and Emanuel (1995a,b).

In section 2 we show how the AB theory can be applied diagnostically. The fundamental assumption of the AB formulation, that the squared local Rossby number $\ll 1$, and its limitations are discussed. The method used for PV inversion is presented, and the incorporation of a frictional boundary layer into the AB theory is described. Section 3 describes the results from calculations where an initially barotropic vortex is placed in a vertical shear flow. The results from the AB calculation are compared with those from the PE calculation. A piecewise PV inversion is performed and used to help interpret the results. In section 4 heating and friction are included in the calculations. The results are summarized and discussed in section 5. Additional discussion of the results, along with technical details of the formulation, can be found in Möller (1995). The results of our comparison between AB and PE solutions suggest that it will be necessary to make a comparison between the nonlinear balanced models and the AB theory. This is the subject of ongoing research that will be reported at a later time.

2. Theoretical details and method of solution

a. Theory

The AB equations set is derived for a cylindrical coordinate system that translates with the vortex (Willoughby 1979). The pressure-based vertical coordinate, z, is the pseudoheight [Eq. (2.1) of Hoskins and Bretherton (1972)]. The mass and wind fields are partitioned into those associated with a translating symmetric vortex (denoted by an overbar) and weak perturbations to this vortex (denoted by a prime). The symmetric vortex, which evolves in time, is in gradient wind balance and is characterized by the potential vorticity $\overline{q}$, the tangential wind $\overline{v}$, the absolute vorticity $\overline{\eta} = f + \overline{\zeta}$, the relative vorticity $\overline{\zeta} = [\partial(r\overline{v})/\partial r]/r$, and the inertia parameter $\overline{\xi} = f + 2\overline{v}/r$, where f is the Coriolis parameter. The symbols used are the same as those in SM.

The fundamental equation of the AB theory is the geopotential tendency equation [(3.10) in SM]. In order to apply the AB theory diagnostically we rewrite the equation in terms of the geopotential tendency, $\partial\phi'/\partial t = \phi'^t$, as

$$\left\{\frac{N^2}{\overline{\overline{q}}\,\overline{\xi}}\frac{1}{r^2}\frac{\partial^2}{\partial\lambda^2} + \frac{1}{r}\frac{\partial}{\partial r}\left[\frac{rN^2}{\overline{\overline{q}}\,\overline{\xi}}\frac{\partial}{\partial r}\right] + \frac{\partial}{\partial z}\left[\frac{\overline{\eta}}{\overline{q}}\frac{\partial}{\partial z}\right] - \frac{1}{r}\frac{\partial}{\partial r}\left[\frac{r}{\overline{q}}\frac{\partial\overline{v}}{\partial z}\frac{\partial}{\partial z}\right]\right\}\phi'^t - \frac{1}{r}\frac{\partial}{\partial z}\left[\frac{r}{\overline{q}}\frac{\partial\overline{v}}{\partial z}\frac{\partial}{\partial r}\right]\phi'^t$$
$$= -\frac{\overline{v}}{r}\frac{\partial}{\partial\lambda}\left\{\frac{N^2}{\overline{\overline{q}}\,\overline{\xi}}\frac{1}{r^2}\frac{\partial^2\phi'}{\partial\lambda^2} + \frac{1}{r}\frac{\partial}{\partial r}\left[\frac{rN^2}{\overline{\overline{q}}\,\overline{\xi}}\frac{\partial\phi'}{\partial r}\right] + \frac{\partial}{\partial z}\left[\frac{\overline{\eta}}{\overline{q}}\frac{\partial\phi'}{\partial z}\right]\right\} - \frac{\overline{v}}{r}\frac{\partial}{\partial\lambda}\left\{-\frac{1}{r}\frac{\partial}{\partial r}\left[\frac{r}{\overline{q}}\frac{\partial\overline{v}}{\partial z}\frac{\partial\phi'}{\partial z}\right] - \frac{1}{r}\frac{\partial}{\partial z}\left[\frac{r}{\overline{q}}\frac{\partial\overline{v}}{\partial z}\frac{\partial\phi'}{\partial r}\right]\right\}$$
$$- \left[\frac{\partial}{\partial r}\left(\frac{N^2}{\overline{q}}\right) - \frac{\partial}{\partial z}\left(\frac{\overline{\xi}}{\overline{q}}\frac{\partial\overline{v}}{\partial z}\right)\right]\frac{1}{r}\frac{\partial\phi'}{\partial\lambda} + \frac{\partial}{\partial z}\left(\frac{\overline{\eta}}{\overline{q}}Q'\right) - \frac{1}{r}\frac{\partial}{\partial r}\left(\frac{r}{\overline{q}}\frac{\partial\overline{v}}{\partial z}Q'\right). \tag{2.1}$$

Here r is the radius, λ the azimuth, N^2 the static stability, ϕ' the perturbation geopotential, and Q' the perturbation heating. The operator on ϕ'^t is a second-order linear operator in r and z and remains elliptic as long as the vortex is symmetrically stable. Balanced models including the AB model require the PV to be positive, that is, the vortex to be symmetrically stable, in order to be able to find a solution.

The derivation of (2.1) is valid as long as the squared local Rossby number, defined by

$$\mathrm{R}_{\mathrm{Ln}}^2 = \frac{n^2\overline{v}^2}{r^2}\Bigg/\left[\overline{\eta\xi} - \frac{\overline{\xi}^2}{N^2}\left(\frac{\partial\overline{v}}{\partial z}\right)^2\right], \qquad (2.2)$$

is small. Note that the square of the azimuthal wavenumber, n, appears in the numerator. SM indicate that the assumption $\mathrm{R}_{\mathrm{Ln}}^2 \ll 1$ can be made only for $n = 1$. Thus the derivations above are valid for the wavenumber-1 asymmetry in the vortex core region, which we shall consider here to be the radii for which the Rossby number Ro $[=\overline{v}/(fr)]$ is greater than unity.

It should be noted that the fundamental assumption of the AB theory may not be strictly satisfied in observed or model vortices. In particular, the squared local Rossby number may not be $\ll$1. In our model calculation it was only possible to investigate situations where $\mathrm{R}_{\mathrm{L}}^2 < 1$ but not $\ll$1. Nevertheless, when $\mathrm{R}_{\mathrm{L}}^2 < 1$ the AB formulation may be considered to be the first term in a series expansion in $\mathrm{R}_{\mathrm{L}}^2$ [see Eq. (3.13) of SM], and an evaluation of the accuracy of AB should be meaningful. A similar evaluation has been made by other investigators of solutions under the quasigeostrophic assumption for Rossby numbers $\sim$⅔ (Rotunno and Bao 1996), $\sim$0.1–1.0 (Keyser et al. 1992), or even $\gg$1 (Hakim et al. 1996), despite that (in principle) there could be substantial errors. In a similar context, McWilliams et al. (1986) found qualitatively apt analogs in quasigeostrophy, despite a moderately large Rossby number. We find, in fact, that the solutions for the fields in the AB formulation converge when $\mathrm{R}_{\mathrm{L}}^2 < 1$ so that an evaluation can be made as to how well the AB formulation represents the PE model solution. On the other hand, when $\mathrm{R}_{\mathrm{L}}^2$ is not $<$1 (or negative!) no such convergent solution can be found (see section 3).

As shown in SM, (2.1) reduces to the linearized quasigeostrophic PV equation for Ro $\to$ 0. Thus the AB theory is valid for all the asymmetric wavenumber components in the outer region or far field, which we shall define as the region for which Ro $<$ 1. In the so-called quasigeostrophic regime certain pairs of higher wavenumbers ($\geq$2) can interact to generate wavenumber 1. Therefore the generalized equation system that extends into the quasigeostrophic regime must include nonlinear interactions. Following SM, the nonlinear terms of the quasigeostrophic PV equation must be added to the right-hand side of the tendency equation in the outer region. Although the terms added are nonlinear, they have no influence on the linearity of the operator on the geopotential tendency itself.

The AB theory assumes that the flow is linear in the vortex core region. This means that the nonlinear terms added to (2.1) should be small in the vortex core. In practice, it turns out that the nonlinearities become dominant near the center of the vortex because the Coriolis parameter f substantially underestimates the inertia frequency in the vortex core region. The largest contribution to the nonlinear terms (SM, p. 3330) scales as $1/f^3$. Thus this term becomes relatively large in the inner core due to f being considerably smaller than the inertia frequency. In a rapidly rotating vortex the inertia stability f^2 has to be replaced by $\overline{\eta\xi}$. As a result, it is necessary to replace f in the nonlinear terms by $\sqrt{\overline{\eta\xi}}$. In the core region, $\sqrt{\overline{\eta\xi}} > f$, so this replacement ensures that the nonlinear terms remain small in the inner core region. In the outer region, $\sqrt{\overline{\eta\xi}} \to f$, so the replacement does not alter the nonlinear terms there. In practice we multiply the nonlinear terms by the factor $f/\sqrt{\overline{\eta\xi}}$. This ''ad hoc'' procedure is consistent with section 5 in SM, where the nonlinear terms are of order $1/\overline{\eta}$ or $1/\overline{\xi}$ (with geometric mean $1/\sqrt{\overline{\eta\xi}}$). The results of the cases described below are, however, changed very little by the inclusion of the nonlinear terms so that the system is, in fact, effectively linear. For this reason we were able to truncate the azimuthal Fourier decomposition at wavenumber 2, neglecting the contribution from higher-order terms.

To ensure that the PV is conserved in the entire domain following the *total* wind, it is necessary to use the PV of the linearized form of the primitive equations. The PV equation can be rewritten in terms of the geopotential ϕ' and its time derivatives as

$$N^2\frac{1}{r}\frac{\partial}{\partial r}\left[\frac{r}{\overline{\xi}}\frac{\partial\phi'}{\partial r} - \frac{1}{\overline{\eta\xi}}\frac{\overline{v}}{r}\frac{\partial^2\phi'}{\partial\lambda^2} \frac{(\partial\overline{v}/\partial z)r}{\overline{\eta\xi q}}\frac{\overline{v}}{r}\left(\frac{\overline{\eta v}}{r}\frac{\partial^3\phi'}{\partial\lambda^2\partial z} - \frac{\partial\overline{v}}{\partial z}\frac{\overline{v}}{r}\frac{\partial^3\phi'}{\partial\lambda^2\partial r} - \overline{\xi}\frac{\partial\overline{v}}{\partial z}\frac{1}{r}\frac{\partial^2\phi'}{\partial\lambda^2}\right)\right]$$
$$- \frac{N^2}{r\overline{q}}\left[-N^2\frac{1}{r}\frac{\partial^2\phi'}{\partial\lambda^2} + \frac{\overline{v}}{r}\frac{\partial^3\phi'}{\partial r\partial\lambda^2} + \frac{\partial\overline{v}}{\partial z}\frac{\overline{v}}{r}\frac{\partial^3\phi'}{\partial z\partial\lambda^2}\right] + \overline{\eta}\frac{\partial^2\phi'}{\partial z^2} - \frac{\partial\overline{v}}{\partial z}\frac{\partial^2\phi'}{\partial r\partial z}$$
$$- \overline{\xi}\frac{\partial\overline{v}}{\partial z}\frac{\partial}{\partial z}\left[\frac{1}{\xi}\frac{\partial\phi'}{\partial r} - \frac{1}{\overline{\eta\xi}}\frac{\overline{v}}{r}\frac{\partial^2\phi'}{\partial\lambda^2} + \frac{\partial\overline{v}/\partial z}{\overline{\eta\xi q}}\frac{\overline{v}}{r}\left(\frac{\overline{v}}{r}\frac{\partial^3\phi'}{\partial\lambda^2\partial z} - \overline{\xi}\frac{\partial\overline{v}}{\partial z}\frac{1}{r}\frac{\partial^2\phi'}{\partial\lambda^2}\right)\right]$$

$$
\begin{aligned}
&= N^2\frac{1}{r}\frac{\partial}{\partial r}\left[\frac{1}{\overline{\overline{\eta\xi}}}\frac{\partial\phi'^{t}}{\partial\lambda} + \frac{(\partial\overline{v}/\partial z)r}{\overline{\overline{\eta\xi q}}}\left(-\overline{\eta}\frac{\partial\phi'^{tt}}{\partial z} - \frac{\overline{\eta v}}{r}\frac{\partial^2\phi'^{t}}{\partial\lambda\partial z}\right)\right]\\
&\quad + N^2\frac{1}{r}\frac{\partial}{\partial r}\left[\frac{(\partial\overline{v}/\partial z)r}{\overline{\overline{\eta\xi q}}}\left(\frac{\partial\overline{v}}{\partial z}\frac{\partial\phi'^{tt}}{\partial r} + \frac{\partial\overline{v}}{\partial z}\frac{\overline{v}}{r}\frac{\partial^2\phi'^{t}}{\partial r\partial\lambda} + \overline{\xi}\frac{\partial\overline{v}}{\partial z}\frac{1}{r}\frac{\partial\phi'^{t}}{\partial\lambda} + \overline{\eta}\frac{\partial Q'}{\partial t}\right)\right]\\
&\quad + N^2\frac{1}{r}\frac{\partial}{\partial r}\left[\frac{(\partial\overline{v}/\partial z)r}{\overline{\overline{\eta\xi q}}}\frac{\overline{v}}{r}\left(-\overline{\eta}\frac{\partial^2\phi'^{t}}{\partial z\partial\lambda} + \frac{\partial\overline{v}}{\partial z}\frac{\partial^2\phi'^{t}}{\partial r\partial\lambda} + \overline{\eta}\frac{\partial Q'}{\partial\lambda}\right)\right]\\
&\quad + \frac{N^2}{r\overline{q}}\left[-\frac{N^2}{\overline{\xi}}\frac{\partial^2\phi'^{t}}{\partial r\partial\lambda} + \frac{\partial\overline{v}}{\partial z}\frac{\partial^2\phi'^{t}}{\partial z\partial\lambda} - \frac{\partial\overline{v}}{\partial z}\frac{\partial Q'}{\partial\lambda}\right] + \overline{\xi}\frac{\partial\overline{v}}{\partial z}\frac{\partial}{\partial z}\left[-\frac{1}{\overline{\overline{\eta\xi}}r}\frac{\partial\phi'^{t}}{\partial\lambda} - \frac{\partial\overline{v}/\partial z}{\overline{\overline{\eta\xi q}}}\left(-\overline{\eta}\frac{\partial\phi'^{tt}}{\partial z}\right)\right]\\
&\quad + \overline{\xi}\frac{\partial\overline{v}}{\partial z}\frac{\partial}{\partial z}\left[-\frac{\partial\overline{v}/\partial z}{\overline{\overline{\eta\xi q}}}\left(-\frac{\overline{\eta v}}{r}\frac{\partial^2\phi'^{t}}{\partial\lambda\partial z} + \frac{\partial\overline{v}}{\partial z}\frac{\partial\phi'^{tt}}{\partial r} + \frac{\partial\overline{v}}{\partial z}\frac{\overline{v}}{r}\frac{\partial^2\phi'^{t}}{\partial r\partial\lambda} + \frac{\overline{\xi}}{r}\frac{\partial\overline{v}}{\partial z}\frac{\partial\phi'^{t}}{\partial\lambda} + \overline{\eta}\frac{\partial Q'}{\partial t}\right)\right]\\
&\quad + \overline{\xi}\frac{\partial\overline{v}}{\partial z}\frac{\partial}{\partial z}\left[-\frac{\partial\overline{v}/\partial z}{\overline{\overline{\eta\xi q}}}\frac{\overline{v}}{r}\left(-\overline{\eta}\frac{\partial^2\phi'^{t}}{\partial z\partial\lambda} + \frac{\partial\overline{v}}{\partial z}\frac{\partial^2\phi'^{t}}{\partial r\partial\lambda} + \frac{\partial\overline{v}}{\partial z}\frac{\overline{v}}{r}\frac{\partial^3\phi'^{t}}{\partial\lambda^2\partial r} + \overline{\eta}\frac{\partial Q'}{\partial\lambda}\right)\right] + q', \qquad (2.3)
\end{aligned}
$$

which can be solved for ϕ' if the operator on ϕ' is elliptic. It can be demonstrated that the neglect of the $O(\mathrm{R}_{\mathrm{L1}}^2)$ terms in the PV equation gives an elliptic operator on ϕ' provided that the vortex is symmetrically stable.

b. PV inversion

The basic idea is to use the AB equations as a diagnostic tool to calculate the balanced asymmetric structure of a PE model calculation. The PE model, which is used to provide the PV for all numerical calculations, is described in Jones and Thorpe (1992). It is a hydrostatic model formulated in Cartesian coordinates, x and y, on an f plane. The vertical coordinate is the same pressure-based height coordinate as in the AB theory. The prognostic variables are the horizontal wind components, u_{zon} and v_{mer}, and the potential temperature, θ. The vertical velocity, w, and the geopotential, ϕ, are diagnosed from the continuity and hydrostatic equations, respectively. Periodic lateral boundary conditions are used for the perturbation fields.

With an azimuthal Fourier decomposition, we obtain the symmetric vortex fields and the wavenumber-1 and wavenumber-2 distributions of the geopotential and the PV from the model data. The inversion is carried out using an iterative method. In order to invert the total PV, (2.1) and the PV equation (2.3) have to be solved simultaneously. The geopotential tendency is obtained from (2.1), which, in operator form, is

$$\phi_1'^{t} = L^{-1}[-O(\phi_1') - \mathrm{NA}(\phi_1', \phi_2') + G(Q_1')], \quad (2.4)$$

where L^{-1} denotes the inverse of the linear operator acting on ϕ'^{t}, O the operator acting on ϕ', and G the operator acting on the heating function Q'. The nonlinear terms of the quasigeostrophic vorticity equation are included in (2.4) through NA, which denotes the nonlinear operator acting on ϕ', where the subscripts 1 and 2 denote the wavenumbers that contribute to wavenumber 1.

Primitive equation model values of ϕ_n' are used as a first guess to solve (2.4) for the geopotential tendency $\phi_n'^{t}$. The PV equation can be written as

$$\phi_n'^{(m+1)} = M^{-1}[q_n' - K(\phi_n'^{t(m)}, \phi_n'^{tt(m)}, Q_n', Q_n'^{t})], \quad (2.5)$$

where $\phi_n'^{(m)}$ denotes the geopotential after the mth iteration, $\phi_n'^{tt}$ the geopotential's second time derivative, $Q_n'^{t}$ the perturbation heating tendency, and M^{-1} the inverse of the linear operator acting on $\phi_n'^{(m+1)}$; q_n' is the PV distribution for azimuthal wavenumber n and K the operator on $\phi_n'^{t(m)}$, $\phi_n'^{tt(m)}$, Q_n', and $Q_n'^{t}$. The procedure for wavenumbers 1 and 2 has to be carried out iteratively. With the wavenumber 1 and 2 components of the PV and the geopotential as a first guess, the tendencies ϕ'^{t} and ϕ'^{tt} for wavenumbers 1 and 2 can be calculated step-by-step as follows:

$$\phi_1'^{t(m)} = L^{-1}[-O(\phi_1'^{(m)}) - \mathrm{NA}(\phi_1'^{(m)}, \phi_2'^{(m)}) + G(Q_1')] \quad (2.6a)$$

and

$$\phi_2'^{t(m)} = L^{-1}[-O(\phi_2'^{(m)}) - \mathrm{NB}(\phi_1'^{(m)}, \phi_1'^{(m)}) + G(Q_2')], \quad (2.6b)$$

where NB denotes the nonlinear operator on $\phi_1'^{(m)}$, the wavenumber-1 component of the geopotential that contributes to the wavenumber-2 component of the geopotential tendency,

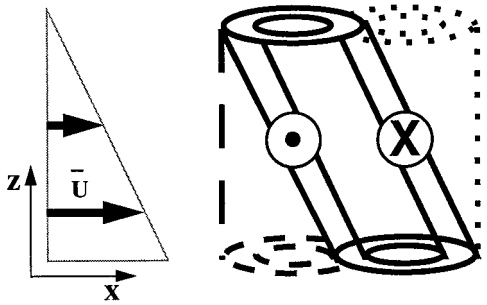

FIG. 2. Schematic showing the influence of vertical shear on an initially barotropic vortex. The shear flow $\overline{U}(z)$ is shown on the left of the figure. The solid black lines on the right of the figure show the PV of the vortex, which has been tilted in the vertical by the action of the vertical shear. The long-dashed lines illustrate the downward projection of the upper-level PV anomaly, resulting in a cyclonic circulation at the surface. The short-dashed lines illustrate the upward projection of the lower-level PV anomaly, giving a cyclonic circulation at upper levels.

$$\phi_1'^{tt(m)} = L^{-1}[-O(\phi_1'^{t(m)}) - \mathrm{NA}(\phi_1'^{(m)}, \phi_2'^{t(m)}) - \mathrm{NA}(\phi_1'^{t(m)}, \phi_2'^{(m)}) + G(Q_1'^{t})] \quad (2.6c)$$

and

$$\phi_2'^{tt(m)} = L^{-1}[-O(\phi_2'^{t(m)}) - \mathrm{NB}(\phi_1'^{(m)}, \phi_1'^{t(m)}) - \mathrm{NB}(\phi_1'^{t(m)}, \phi_1'^{(m)}) + G(Q_2'^{t})]. \quad (2.6d)$$

Using the tendencies ϕ'^{t}, ϕ'^{tt} obtained in this way and the given PV from the PE model, it is possible to calculate the $(m + 1)$th guess for wavenumber 1 and 2 components of the new geopotential ϕ' from (2.5) with $n = 1$ and $n = 2$ respectively. The iterative method was applied with the use of underrelaxation, without which the system failed to converge.

The required translation velocities and accelerations of the coordinate system are calculated from the PE model from the positions of the geopotential minimum at the analysis time and 3 h before and after, whereas the time derivatives of the acceleration, $\ddot{c}_x$ and $\ddot{c}_y$, turned out to be negligible. Once we have the balanced perturbation geopotential and the geopotential's first and second time derivatives, we can calculate the perturbation wind components u', v', and w' from (3.7)–(3.9) of SM.

c. Incorporation of friction in the AB theory

In order to incorporate a frictional boundary layer in the theory, the momentum, PV, and geopotential tendency equations must be suitably modified. Observations show that surface momentum fluxes can be represented by the "bulk aerodynamic formula." If the boundary layer influence is taken into account by integration of the momentum equations from the surface to the top of the boundary layer at $z = h$, the friction term in the momentum equations in a translating cylindrical coordinate system is given by

$$-\frac{C_D}{h}[(u + c_r)^2 + (v + c_\lambda)^2]^{1/2}(\mathbf{u} + \mathbf{c}_{\mathrm{cyl}}), \quad (2.7)$$

where C_D denotes the nondimensional drag coefficient for sea surface stress, u and v are the storm-relative radial and tangential velocity components, respectively, $\mathbf{u}$ is the corresponding velocity vector, $\mathbf{c}_{\mathrm{cyt}} = (c_r, c_\lambda)$ is the translation velocity, and c_r and c_λ the radial and azimuthal velocity components. There are several empirical determinations of C_D, which are all of order 1.5×10^{-3} (Roll 1965; Miller 1964). In order to include the drag coefficient in the AB theory, (2.7) has to be linearized using the assumption that the asymmetries are much smaller than the symmetric components. Although the symmetric radial wind, $\overline{u}$, may not be small compared with $\overline{v}$ in the boundary layer (e.g., Smith

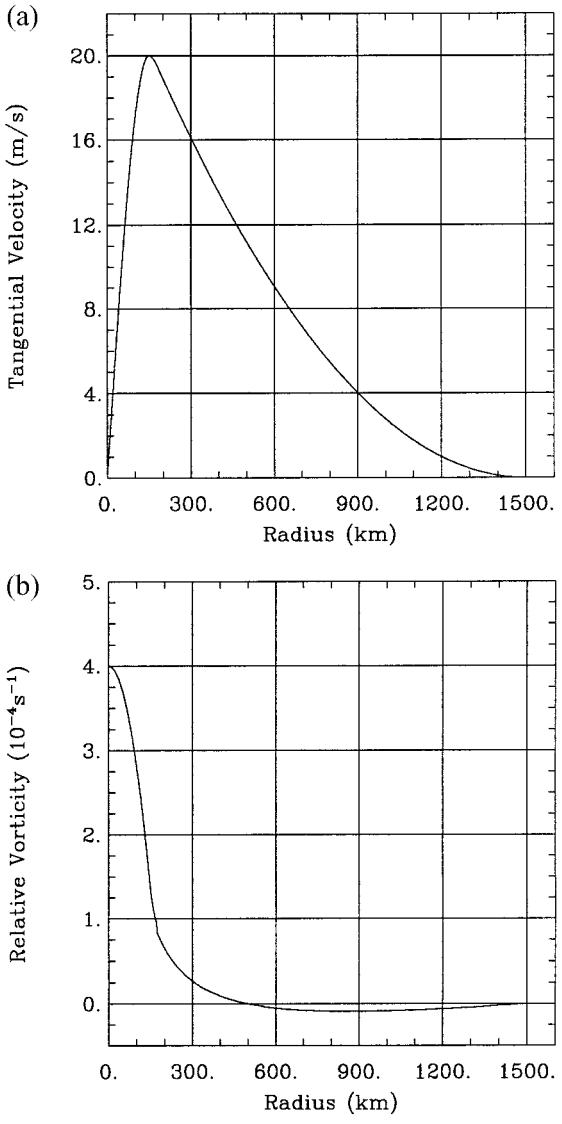

FIG. 3. Radial profile of (a) the tangential velocity and (b) the relative vorticity of the initial vortex in section 3.

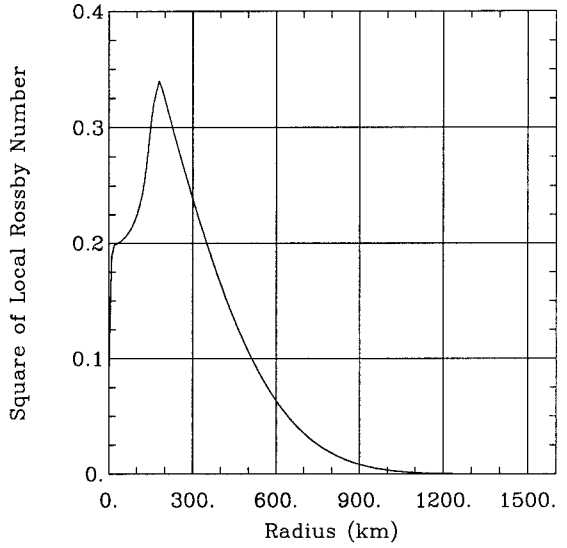

FIG. 4. Radial profile of the squared local Rossby number of the initial vortex.

1968), $\overline{u}$ is assumed here to be much smaller than the tangential wind, $\overline{v}$ (Anthes 1982; Houze 1993). This assumption is necessary for the AB formulation. The translation velocity has the same order of magnitude as the perturbation velocity and is treated accordingly in the linearization.

Applying the foregoing assumptions, we can incorporate the frictional drag in the AB theory. In the boundary layer, the drag expressions

$$v\text{drag} = \frac{1}{\overline{\eta}\overline{\xi}}\left[\overline{\eta} D_r c_r - D_\lambda \frac{D_v c_\lambda}{Dt} - \frac{D_r}{r}\frac{\partial \phi'}{\partial \lambda} - D_r D_\lambda c_\lambda\right] \tag{2.8a}$$

and

$$u\text{drag} = \frac{1}{\overline{\eta}\overline{\xi}}\left[-\overline{\xi} D_\lambda c_\lambda - D_r \frac{D_v c_r}{Dt} - D_\lambda \frac{\partial \phi'}{\partial r} - D_r D_\lambda c_r\right] \tag{2.8b}$$

have to be included in the momentum equations, the geopotential tendency equation, and in the PV equation. The drag coefficients, D_r and D_λ, are defined as follows:

$$D_r = \left(\frac{C_D}{h}\right)(\overline{v}^2)^{1/2}, \qquad D_\lambda = \left(\frac{C_D}{h}\right)2(\overline{v}^2)^{1/2}.$$

In the case of the momentum equations, the drag expressions (2.8a) and (2.8b) have simply to be added to the tangential and radial velocity [SM (3.7) and (3.8)] respectively. In the case of the geopotential tendency equation, it is necessary to add

$$\frac{1}{r}\frac{\partial (ru\text{drag})}{\partial r} + \frac{1}{r}\frac{\partial v\text{drag}}{\partial \lambda}, \tag{2.9}$$

to (2.1), which is derived from the continuity equation [SM(3.4)]. The following term

$$N^2\left(\frac{1}{r}\frac{\partial (rv\text{drag})}{\partial r} - \frac{1}{r}\frac{\partial u\text{drag}}{\partial \lambda}\right) \tag{2.10}$$

has to be added to the PV equation, where the radial and tangential velocity components appear in the relative vorticity ζ.

3. Initially barotropic vortex in a vertical shear flow

a. Primitive equation calculation

In this section the PE model is applied without heating and friction and initialized with a vertical shear flow given by

$$\overline{U}_A = U_0 + U_z z,$$

where U_0 (=5 m s^{-1}) and U_z (=-5×10^{-4} s^{-1}) are constants. This zonal flow is in thermal wind balance with a horizontal temperature gradient. The stably stratified temperature field has a constant static stability $N^2 = 1.5 \times 10^{-4}$ s^{-2}. The latitude is 20° N, so that $f = 5 \times 10^{-5}$ s^{-1}. Since the shear, static stability, and Coriolis parameter are all constant, this flow has uniform potential vorticity. The domain is 6480 km in the x direction and 5760 km in the y direction with a horizontal resolution of 15 km. The vertical resolution is 2 km and the domain height is 10 km.

Figure 2 illustrates what happens when an axisymmetric barotropic vortex (from Willoughby 1988) is superimposed on this initial state. In response to the vertical shear, the vortex tilts in the plane of the shear. Associated with the tilt there is an upward and downward projection of the PV anomalies due to the lower- and upper-level vortices respectively. The projections, illustrated by the dashed lines in Fig. 2, lead to wavenumber-1 flow asymmetries. Jones (1995) attributes the observed cyclonic rotation of the upper- and lower-level vortices about the midlevel center to advection by these flow asymmetries. The axisymmetry of the vortex is distorted among other things by the divergent circulation of the vortex. The tilt, the upward and downward projection of the PV anomalies, and the distortion of the vortex appear in a cylindrical coordinate system as a wavenumber-1 distribution. After 24 h the vortex moves about 200 km to the east.

Figure 3 shows the radial profile of the tangential wind, $\overline{v}$, and the relative vorticity distribution of the initial vortex. The magnitudes of the relative vorticity and $\overline{v}$ are important, as they determine the size of the local Rossby number squared R_L^2 [(2.2), from now on omitting subscript 1 for notational convenience], in which the absolute vorticity is in the denominator. If, for example, the relative vorticity becomes negative, or if $\overline{v}$ is very anticyclonic, then R_L^2 can become large enough to invalidate the assumption in the AB theory

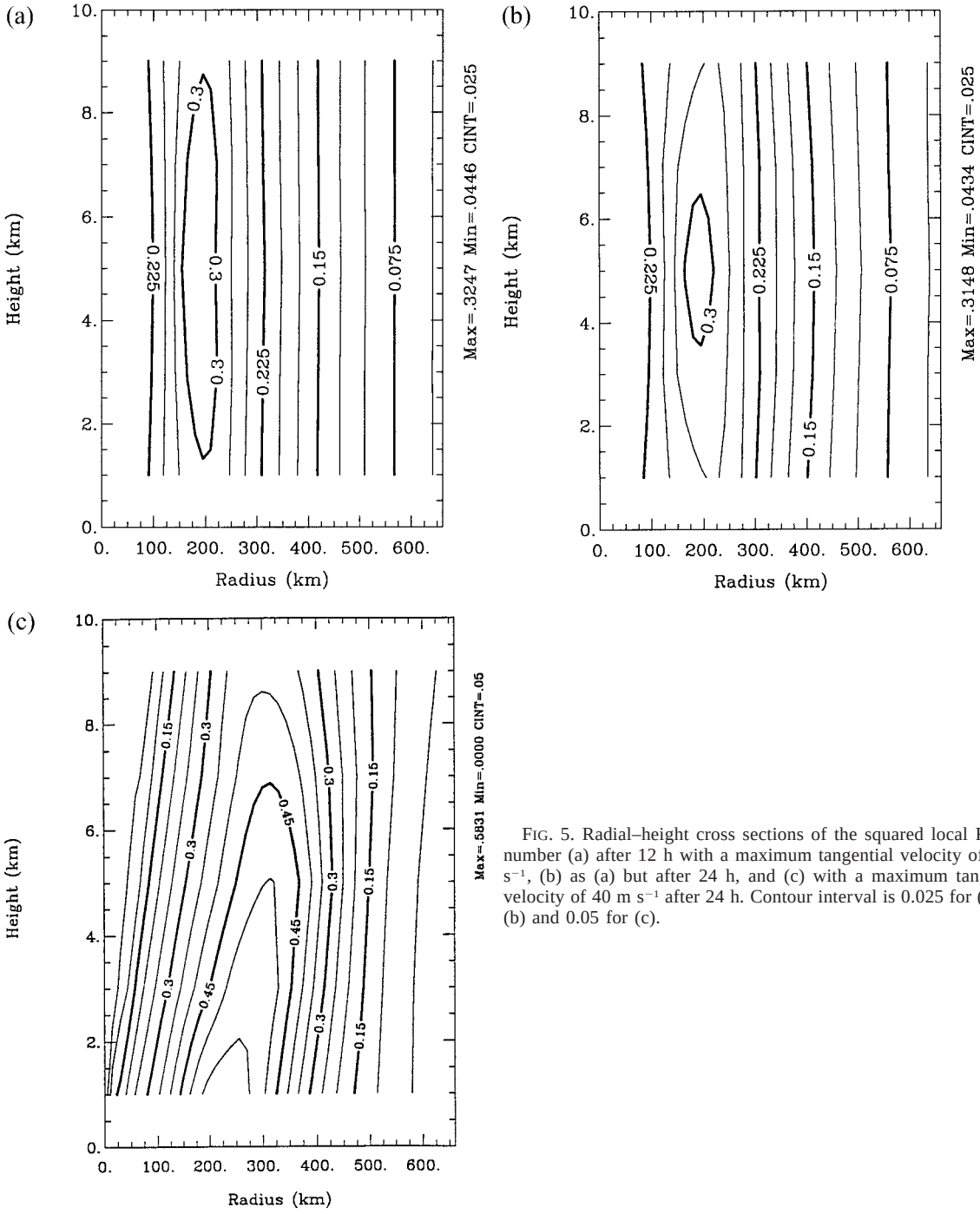

FIG. 5. Radial–height cross sections of the squared local Rossby number (a) after 12 h with a maximum tangential velocity of 20 m s^{-1}, (b) as (a) but after 24 h, and (c) with a maximum tangential velocity of 40 m s^{-1} after 24 h. Contour interval is 0.025 for (a) and (b) and 0.05 for (c).

that $R_L^2 \ll 1$. For the vortex profile used below the relative vorticity of the vortex remains positive inside a radius of 500 km, which is the domain of interest. The radial profile of the local Rossby number squared at the initial time and cross sections of R_L^2 at 12 and 24 h are shown in Figs. 4, 5a, and 5b. Note that R_L^2 has a maximum of about 0.3 at a radius of 200 km and a height of 5 km. Using a vortex with $\overline{v}$ twice as large (maximum $\overline{v} = 40$ m s^{-1}), R_L^2 has a maximum of about 0.6 after 24 h at a radius of 200 km (Fig. 5c).

The PV of the PE model is calculated at 12 and 24 h using the vortex with maximum $\overline{v} = 20$ m s^{-1}. Figures 6a and 6b show the cyclonic rotation of the upper- and lower-level vortices about the midlevel center marked by the cyclone symbol. A line passes through the PV maximum at the top and bottom, showing the orientation

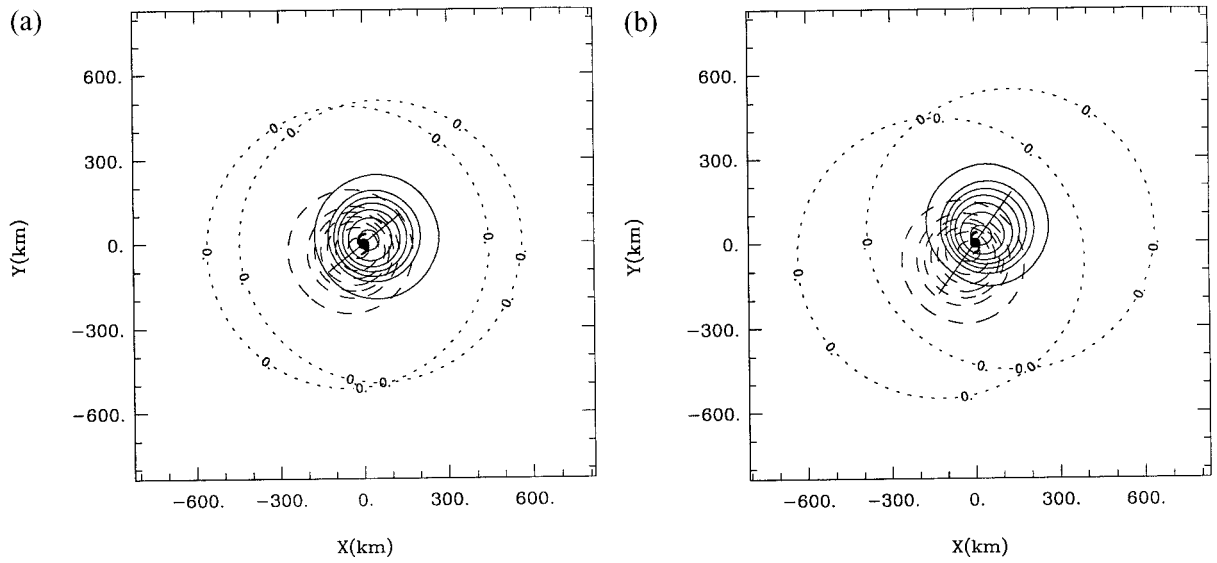

FIG. 6. Horizontal cross sections of the upper- and lower-level density-weighted potential vorticity fields. The density-weighted potential vorticity of the background flow has been subtracted. The solid contours are for $z = 2$ km, the dashed contours for $z = 8$ km. In both cases the zero line is dotted. Contour interval is 0.25×10^{-6} m^2 K/(s kg). The position of minimum perturbation geopotential at $z = 5$ km is marked by a cyclone symbol. Only a portion of the model domain is shown: (a) 12 h and (b) 24 h. The solid line shows the orientation of the tilt.

of the tilt. After 12 h the upper-level PV anomaly is southwest of the lower PV anomaly, and after 24 h there is a larger north–south component to the tilt and the separation of the centers of the upper and lower anomalies has increased.

Since the environmental flow in the present calculation contains vertical shear, the vortex translation speed, **c**, is different at each level and we assume that the vortex moves with the speed of the vortex center at a height of 5 km. At 12 and 24 h the zonal speed is $c_x = 2.5$ m s^{-1}, and the meridional speed is $c_y = -5.0 \times 10^{-3}$ m s^{-1} (effectively zero). The corresponding accelerations are $\dot{c}_x = 1.7 \times 10^{-6}$ m s^{-2} and $\dot{c}_y = 1.8 \times 10^{-6}$ m s^{-2}. In principle, the determination of the translation speed can be problematic if **c** is different at each level, since it is then necessary to find the most appropriate level for the choice of **c**. In practice it turns out that in the baroclinic experiment described here the choice of the translation speed was not overly sensitive to the choice of the level. The reason lies in the weak tilt of the vortex so that the differences between the translation speed at each level would imply a horizontal displacement less than the horizontal grid length. With a stronger shear or a narrower vortex profile, the sensitivity to the choice of level used to define **c** would increase.

b. Comparison with AB theory

Compared with the conventional balanced equations (McWilliams 1985), the AB theory is a new theory, and as far as we are aware, the equations have not yet been solved in three dimensions. A good test of the theory is to compare the structure of the AB balanced fields with those obtained directly from the primitive equations. In the PE calculation in this section, the divergence is small and the wind and mass fields are broadly in balance. Thus, the PV inversion using the AB theory should be able to reproduce the height and wind fields obtained from the PE model within the restrictions imposed by the size of the squared local Rossby number.

As an example, Figs. 7 and 8 compare the wavenumber-1 distributions of the tangential and radial velocities from the AB and PE models at 12 h and at heights of 2 and 8 km. Figure 9 shows the vertical velocity at heights of 4 and 6 km, the levels at which the values are a maximum and, in the case of the PE model, equal. The radial and tangential velocity components of the AB model (u'_{AB} and v'_{AB}) agree very well in amplitude and in the orientation of the inner region with the analogous PE velocities (u'_{PE} and v'_{PE}) at a height of 8 km. The agreement at a height of 2 km is reasonable. The radial velocity shows a typical wavenumber-1 pattern with the extrema orientated east–west; the extrema of the tangential velocity are orientated north–south. The patterns in the outer region show that the amplitudes in the AB calculation are higher than in the PE calculation. At a height of 2 km, the maximum of u'_{PE} is 7.2 m s^{-1} in the inner region (Fig. 7a) compared with $u'_{AB} = 10.0$ m s^{-1} (Fig. 7b); at a height of 8 km the corresponding values are $u'_{PE} = 2.7$ m s^{-1} (Fig. 7c) and $u'_{AB} = 2.6$ m s^{-1} (Fig. 7d). At a height of 2 km, the maximum of v'_{PE} is 6.8 m s^{-1} in the inner region (Fig. 8a) compared with $v'_{AB} = 9.8$ m s^{-1} (Fig. 8b); at a height of 8 km the corresponding values are $v'_{PE} = 2.5$ m s^{-1} (Fig. 8c) and $v'_{AB} = 3.2$ m s^{-1} (Fig. 8d). The extrema of the vertical

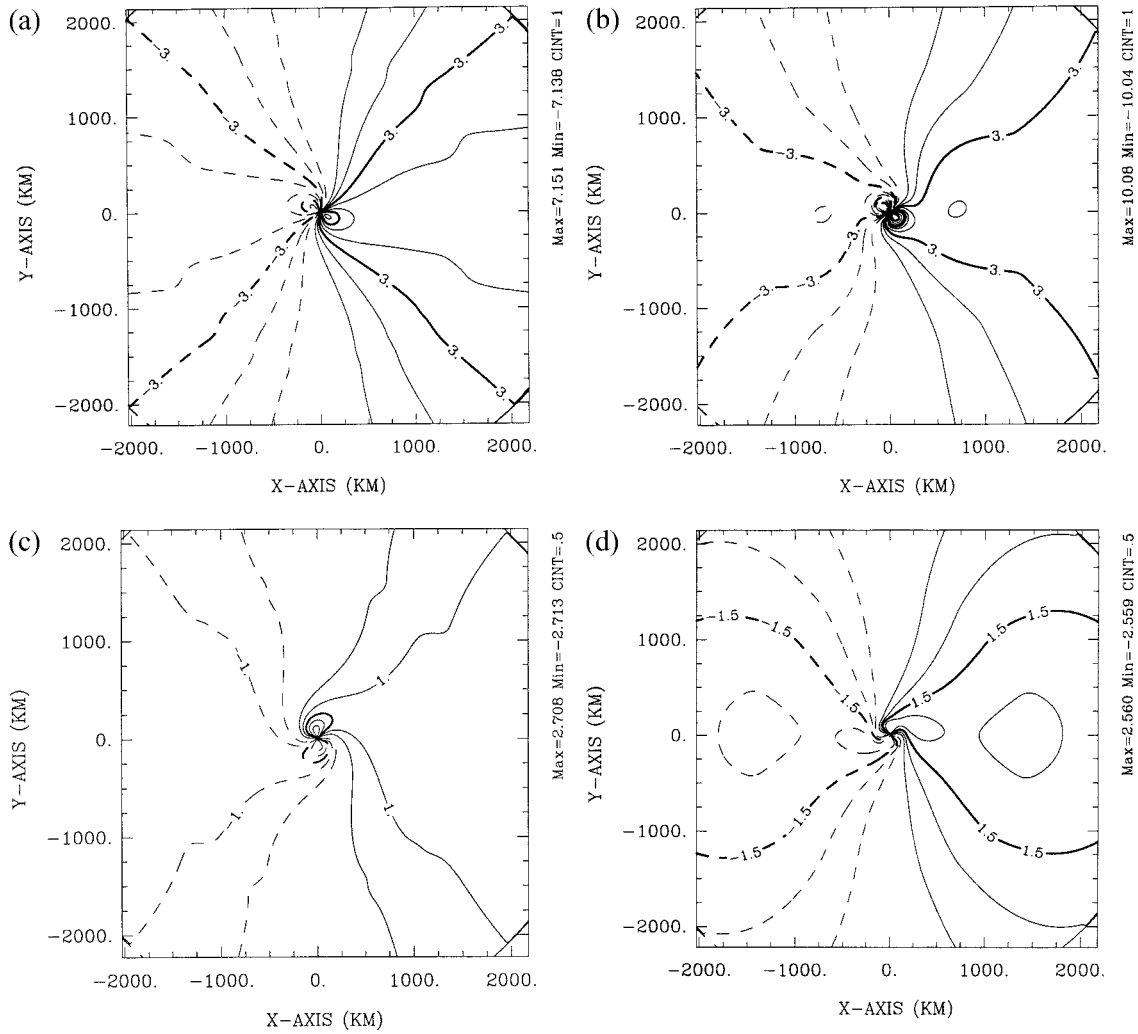

FIG. 7. Horizontal cross sections of the wavenumber 1 component of the radial velocity u after 12 h (a) at a height of 2 km (calculated with the PE model), (b) at a height of 2 km (calculated with the AB model), (c) at a height of 8 km (calculated with the PE model), and (d) at a height of 8 km (calculated with the AB model). Contour interval is 1.0 m s^{-1} for (a) and (b) and 0.5 m s^{-1} for (c) and (d). Here (0 km, 0 km) is the vortex center; this corresponds to (−360 km, −15 km) in x–y space.

velocity of the PE (w'_{PE}) and AB (w'_{AB}) models are orientated northwest–southeast. At a height of 4 and 6 km $w'_{PE} = 0.049$ m s^{-1} (Fig. 9a) and the corresponding $w'_{AB} = 0.054$ m s^{-1} at a height of 6 km (Fig. 9b) and 0.074 m s^{-1} at a height of 4 km (Fig. 9c). The calculation at 24 h gives a very similar result (not shown).

The relative error between the amplitude maxima of the velocities in the AB and PE calculations is, as expected, comparable with the maximum R_L^2, which is here 0.33 at lower levels. The deviation between the results is even more significant if we use the vortex profile with maximum $\overline{v} = 40$ m s^{-1}, where the maximum of $R_L^2 = 0.6$ after 24 h (Fig. 5c). The vertical velocity w'_{AB} (not shown), for example, differs from w'_{PE} (also not shown), particularly near the bottom of the domain. At a height of 4 and 6 km, the maximum of w'_{PE} is 0.14 m s^{-1} compared with $w'_{AB} = 0.31$ m s^{-1} at a height of 4 km and $w'_{AB} = 0.16$ m s^{-1} at a height of 6 km. The maxima of the asymmetries calculated from the PE model are orientated east–west in the inner region, whereas the orientation from the AB model calculations is more north–south at each level. Near the lower part of the domain, the vertical velocity in the AB solution is twice as large as that in the PE calculation. The maximum error in w lies between 200- and 300- km radius, exactly where the local Rossby number has its maximum. This suggests that the AB solution is less accurate where the local Rossby number is large and that R_L^2 can be used as an indicator for the error in w.

c. Piecewise inversion

To understand the influence of vertical shear on the vortex and the corresponding PV distribution, it is help-

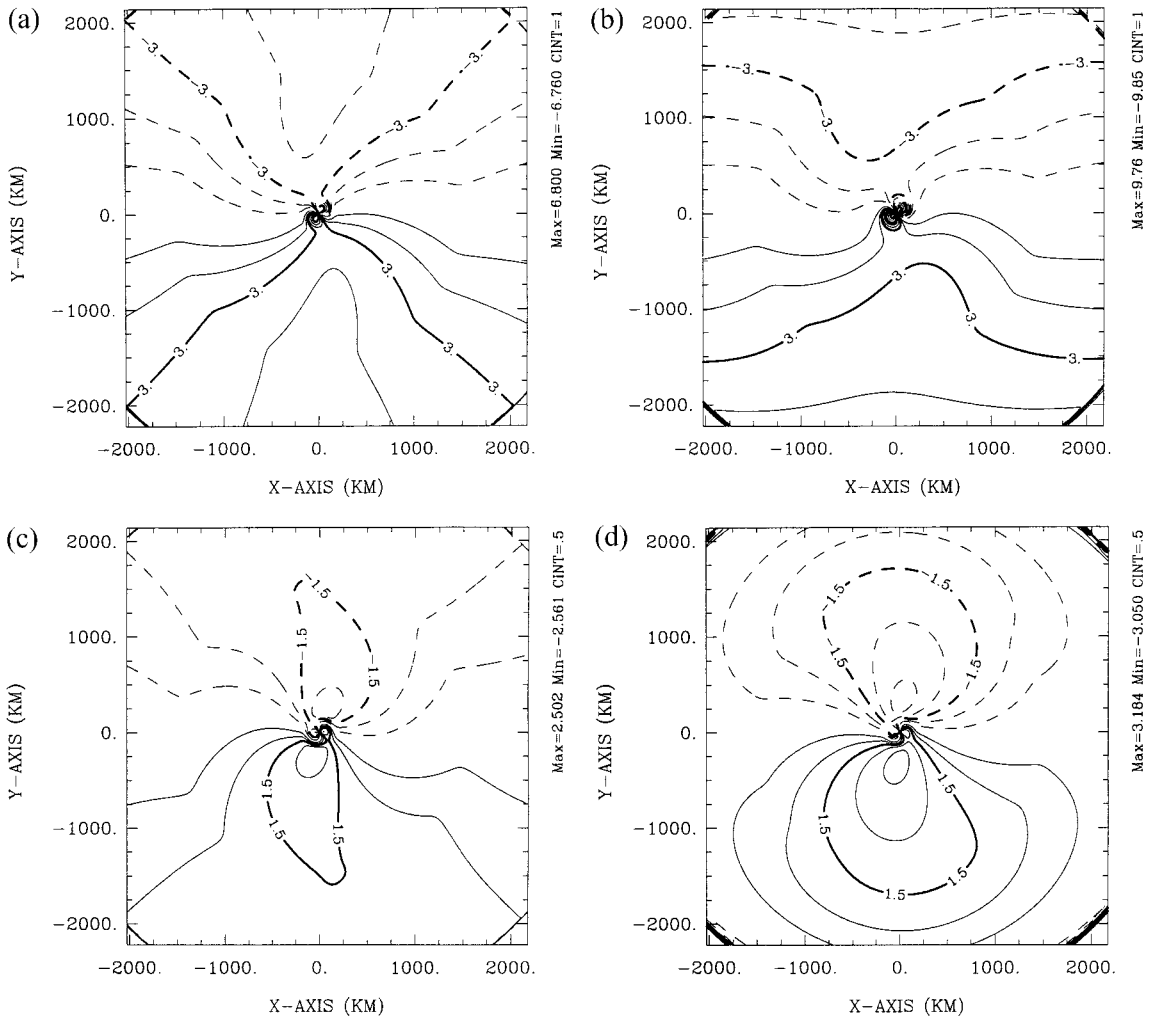

FIG. 8. As in Fig. 7 but for the tangential velocity v.

ful to transform the radial and tangential velocity fields into the corresponding zonal and meridional wind fields. Figure 10 shows the wavenumber-1 contributions to the horizontal wind vectors obtained from the AB calculation at heights of 2 and 8 km at 12 and 24 h. At 2 km at 12 h, the flow is from northwest to southeast in the region where the PV anomaly is positive, while at 8 km it is mainly from the southwest. After 24 h the direction of the flow across the center changes, as the vortex rotates further cyclonically. We assume that the motion of the PV anomalies occurs due to advection by the balanced part of the wind field associated with the wavenumber-1 component of the PV anomaly. Under this assumption the wind fields shown should contain components that account for both the translation and rotation. It should be possible to isolate the wind field responsible for the rotation by calculating the wind field in the translating coordinate system. Figure 11 shows the flow at 12 h in the translating system. This flow would tend to advect the surface vortex southeastward and the upper-level vortex northwestward, resulting in an anticyclonic rotation of the upper- and lower-level vortices about the midlevel center. The apparent inconsistency with the cyclonic rotation seen in Fig. 6 is resolved by performing a piecewise PV inversion as described below.

Piecewise PV inversion (Davis 1992) is a useful method for diagnosing the contributions to the total flow from individual portions of the PV distribution. Piecewise inversion has been applied to interpret baroclinic instability (Robinson 1989) as well as observations (Robinson 1988; Davis and Emanuel 1991). Davis (1992) pointed out that piecewise PV inversion is unique only for a linear inverse operator such as that in the quasigeostrophic theory. Unfortunately, quasigeostrophy is valid for large-scale motions only and becomes inaccurate for large Rossby numbers. Davis noted the ambiguity of the nonlinearity in the inversion operator for the more general Ertel PV (Ertel 1942), which is used in the standard nonlinear balance system. Thorpe

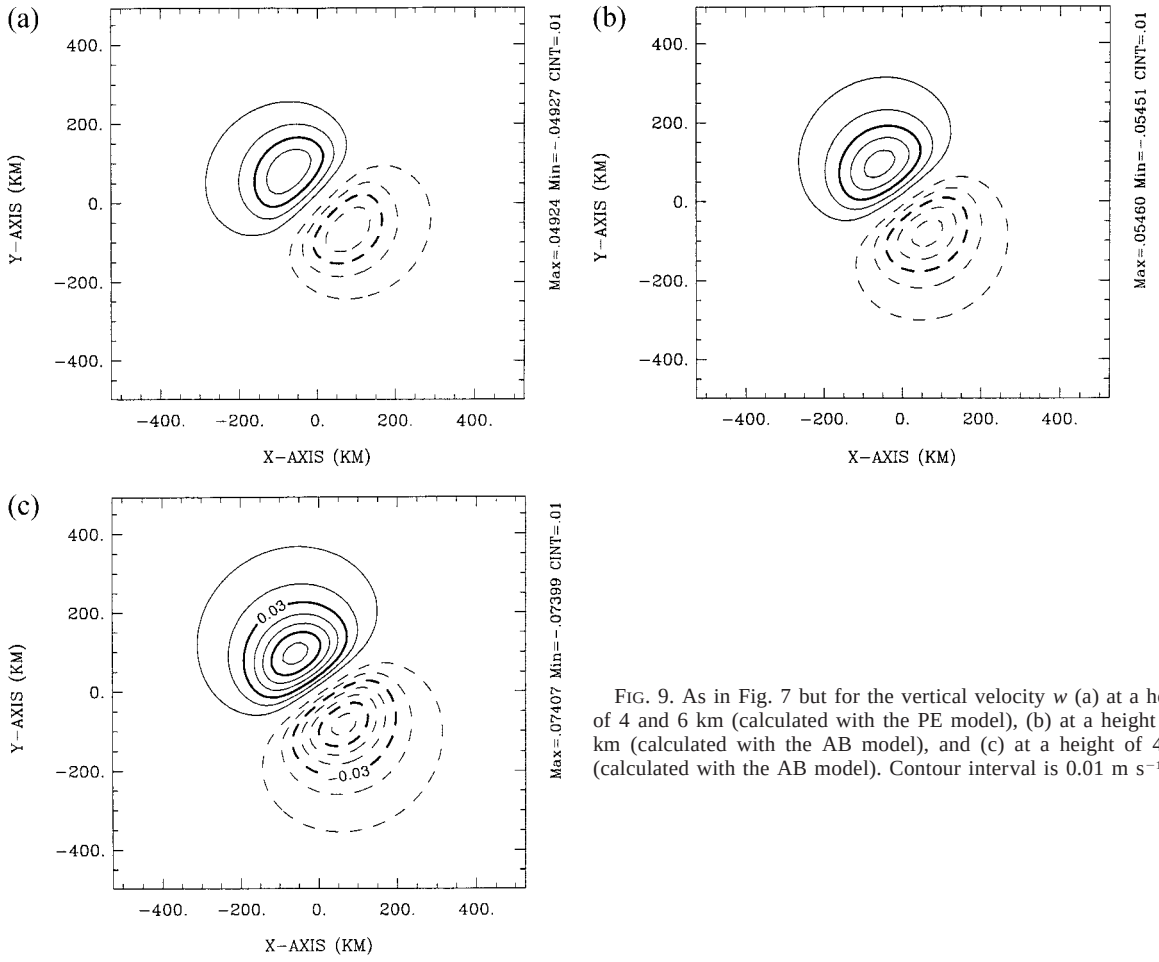

FIG. 9. As in Fig. 7 but for the vertical velocity w (a) at a height of 4 and 6 km (calculated with the PE model), (b) at a height of 6 km (calculated with the AB model), and (c) at a height of 4 km (calculated with the AB model). Contour interval is 0.01 m s^{-1}.

and Bishop (1995) note also that linear superposition does not carry over to Ertel PV, though they hypothesize that the nonlinearity should not be significant except for anomalies that are very close together. In contrast to other balance theories (e.g., the nonlinear balance, and the semi- or quasi-balance [Raymond 1992] approximations), the AB theory has the advantage of being effectively linear (in the case presented here) and also of being able to handle large Rossby numbers Ro and large divergence. The following results will show how the AB theory can be used easily to invert the PV anomalies obtained from the PE model piecewise.

We investigate the PV-induced horizontal circulation at the top and bottom of the domain independently by dividing the PV anomaly into an upper- and a lower-level "piece." In contrast to the inversion of the PV of the full domain, where the outer boundary is specified from the observed geopotential, the piecewise method dictates that the geopotential has to be set to zero. When considering the upper (lower)-level piece of PV, the vertical derivatives of the geopotential (i.e., the temperature) are set to zero at the bottom (top) of the domain. This is necessary because we have no way of ascertaining what portion of the observed geopotential should be associated with a given piece of PV anomaly. The lateral boundaries are assumed to be far enough away from the area of interest that the boundary conditions do not affect the result. If we set the PV anomaly in the upper region to be zero, we are able to calculate at each level the horizontal winds induced by the lower PV anomaly and vice versa. If we add the pieces of the resulting wind vectors together we should obtain the same answer as if we inverted the total PV anomaly.

The lower-level piece is defined at 0, 2, and 4 km, the upper-level piece at 6, 8, and 10 km. Figure 12 shows the winds at a height of 2 and 8 km from the piecewise PV inversion after 12 h. All results are obtained from the AB model in the translating coordinate system in order to show the influence of the PV anomalies, independently of the translation. Figures 12a and 12b show the influence of the upper-level PV anomaly at 8 and 2 km, respectively. The PV anomaly induces a southeasterly flow with a maximum of $\mathbf{v} = 3.8$ m s^{-1} (Fig. 12a) at 8 km and a maximum of $\mathbf{v} = 0.9$ m s^{-1} (Fig. 12b) at 2 km. Figures 12c and 12d show the influence of the lower-level PV anomaly at 8 and 2 km,

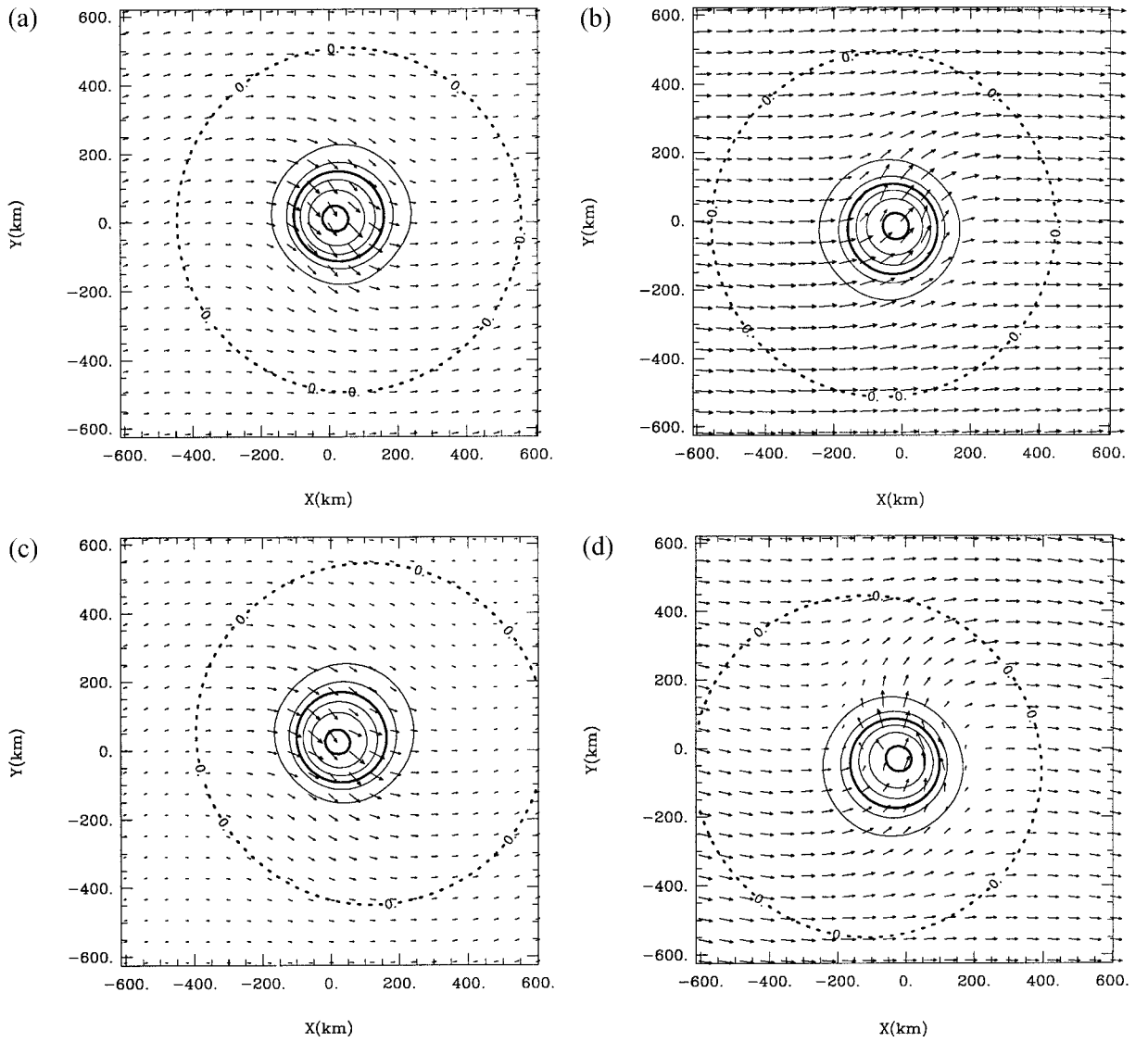

FIG. 10. Horizontal cross sections calculated with the AB model. Arrows indicate the wavenumber-1 component of the horizontal wind. Contours of potential vorticity with contour interval 0.25×10^{-6} m^2 K/(s kg) (a) at a height of 2 km at 12 h, maximum vector is 11.1 m s^{-1}; (b) as in (a) but at a height of 8 km, maximum vector is 3.4 m s^{-1}; (c) at a height of 2 km at 24 h, maximum vector is 16.3 m s^{-1}, and (d) as in (c) but at a height of 8 km, maximum vector is 3.7 m s^{-1}. Here, (0 km, 0 km) is the midlevel vortex center.

respectively. The PV anomaly induces a northwesterly flow with a maximum of $\mathbf{v} = 0.8$ m s^{-1} (Fig. 12c) at 8 km and a maximum of $\mathbf{v} = 9.5$ m s^{-1} (Fig. 12d) at 2 km. Combining the flow at 2 km, induced by the upper- and lower-level PV anomalies, we obtain a northwesterly flow with a maximum of $\mathbf{v} = 8.6$ m s^{-1} (Fig. 13a). At 8 km we obtain a southeasterly flow with a maximum of $\mathbf{v} = 3.0$ m s^{-1} (Fig. 13b). A comparison between the combined flow at a height of 2 km (Fig. 13a) and the flow at 2 km, which is obtained from the total PV anomaly (Fig. 11a), shows there is very good agreement. The same is true for the height of 8 km (Figs. 11b and 13b).

To interpret these results we concentrate on the 2-km level. Analogous arguments can be used to interpret the results at 8 km. The total flow across the PV center has the opposite sign to that one would expect from the rotation. Figure 12d shows a northwesterly flow induced by the low-level PV anomaly and which is dominant. The weaker southeasterly flow associated with the upper-level PV anomaly would explain the observed cyclonic rotation of the upper and lower vortices around the midlevel center (Fig. 12b). The flow associated with the low-level PV anomaly can be explained as follows. In our calculation we use the midlevel geopotential to define the vortex center. This center lies midway between the upper- and lower-level PV maxima (Fig. 6a). The lower-level wavenumber-1 asymmetry of PV arises due to the different location of the center and the PV

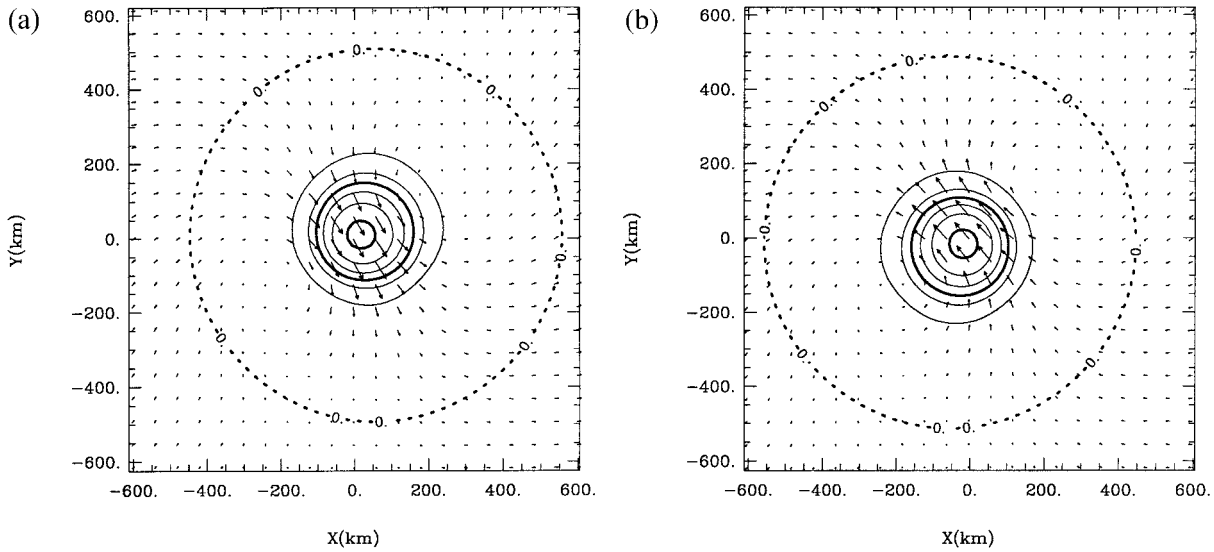

FIG. 11. Horizontal cross sections in the translating coordinate system calculated with the AB model at 12 h. Arrows indicate the wavenumber-1 component of the horizontal wind. Contours of potential vorticity with contour interval 0.25×10^{-6} m^2 K/(s kg) (a) at a height of 2 km and maximum vector of 8.5 m s^{-1}, and (b) at a height of 8 km and maximum vector of 3.4 m s^{-1}. Here, (0 km, 0 km) is the midlevel vortex center.

maximum. This asymmetry would essentially vanish if the vortex center coincided with the position of the lower-level PV maximum. Thus, the northwesterly flow seen at 2 km due to the lower-level PV anomaly is an artifact of the choice of the vortex center and is not physical. This flow is always in the opposite sense to the direction of the rotation and itself will rotate cyclonically around the midlevel center. In contrast, the flow at 2 km associated with the upper-level PV anomaly is due to the vortex tilt, which gives a horizontal displacement between the upper- and lower-level PV anomalies. If the vortex center coincided with the PV maximum at 2 km, the flow across the vortex center due to the upper-level anomaly would not disappear, but would be strengthened. Therefore we conclude that the large-scale rotation results from the wind field associated with the upper-level PV anomaly (Fig. 12b).

Only with the piecewise inversion is it possible to isolate the effect of the influence of the upper-level PV anomaly. If the symmetric vortex is tilted in the vertical, the decomposition of the flow depends on the choice of level one uses for defining the center. We chose the midlevel center so that the sum of each piece added up to the total flow. In doing so we neglected part of the contribution from the symmetric part of the upper-level PV anomaly, which also contributes to the rotation of the low-level vortex. Piecewise PV inversion is a useful tool for studying vortex dynamics. We have demonstrated that the AB theory can be used to perform a piecewise inversion. If attention is paid to the choice of the vortex center, piecewise inversion can be used to understand the vortex motion. The application of this tool to further datasets and further investigation of the significance of the choice of vortex center is a subject for future work.

d. Comparison with quasigeostrophic theory

The quasigeostrophic theory is unable to represent the vortex core region. To confirm this we compare the velocities obtained from the PE model with those calculated diagnostically using the quasigeostrophic theory at 12 h. For both the radial and tangential velocities, u'_{qg} and v'_{qg}, where the subscripts ''qg'' denote the quasigeostrophic approximation, the orientation of the extrema of the wavenumber-1 distributions (not shown) is similar to that of the PE model. The amplitude in the center, however, is at 2 km about three times larger and at 10 km about nine times larger than in the PE calculation. At a height of 2 km, u'_{qg} has a maximum of 27 m s^{-1} and v'_{qg} a maximum of 26 m s^{-1}. The maxima at a height of 8 km are for both u'_{qg} and v'_{qg} 18 m s^{-1}. Comparing the deviations of the AB theory and of the quasigeostrophic assumption with the PE calculations gives the following: at 2 km a 280% error for u'_{qg} and v'_{qg}; the error in the AB theory, by contrast, is 41% for u'_{ab} and 43% for v'_{ab}. At 8 km the error for u'_{qg} and v'_{qg} is about 600%, whereas u'_{ab} deviates by 5% and v'_{ab} by 27% from the corresponding PE values. These results confirm that in the vortex core region, the quasigeostrophic assumption is invalid, whereas the AB theory gives qualitatively good results at lower levels and a very good agreement at upper levels. As the quasigeostrophic approximation assumes the vertical advection and divergence to be small, it would be expected that errors made using this approximation would be even

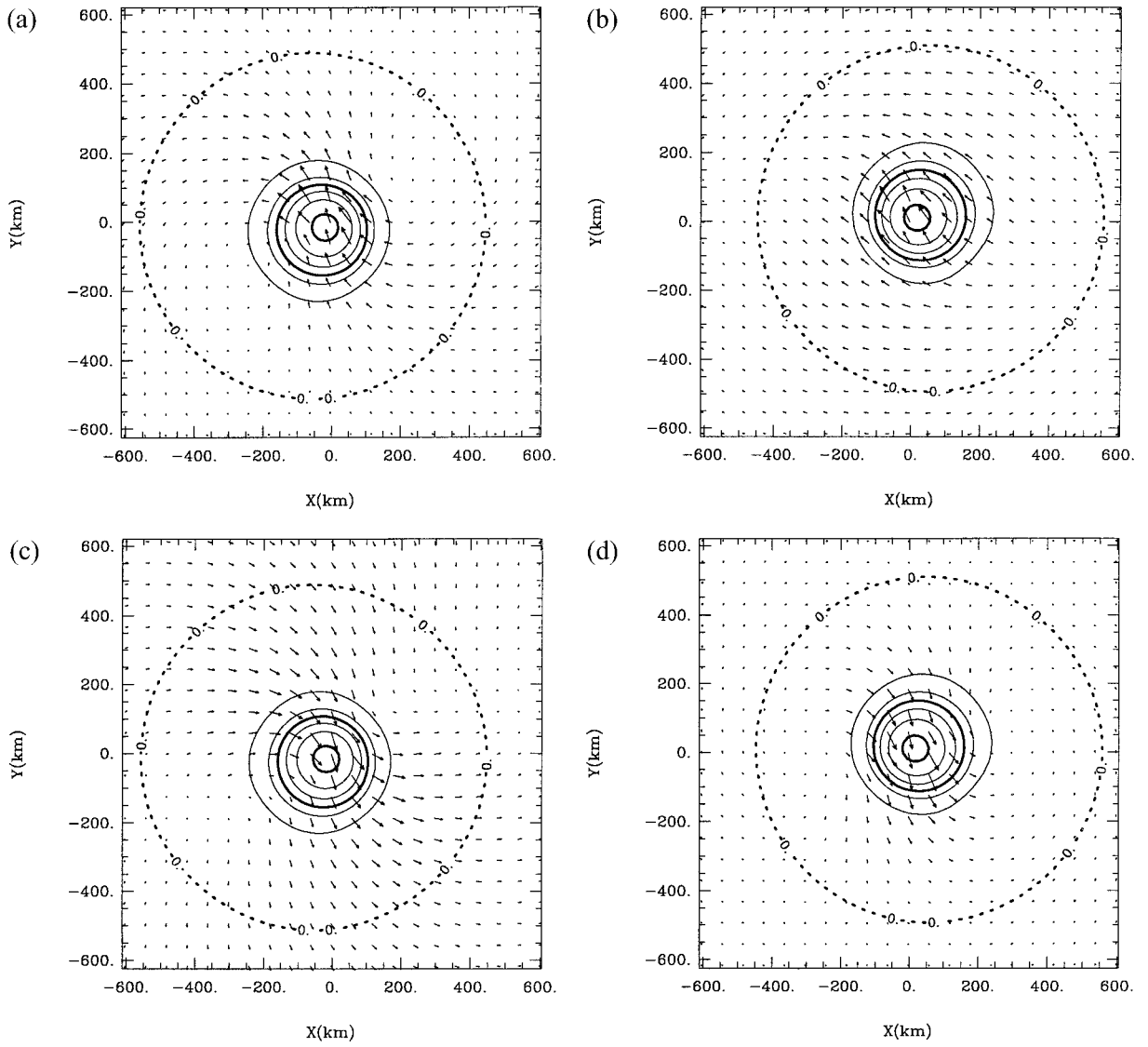

FIG. 12. Horizontal cross sections at 12 h using piecewise inversion. Arrows indicate the wavenumber 1 component of the horizontal wind. Contours of potential vorticity at the same level as the arrows with contour interval 0.25×10^{-6} m^2 K/(s kg) (a) at a height of 8 km, induced by the upper-level PV anomaly, maximum vector is 3.8 m s^{-1}; (b) at a height of 2 km, induced by the upper-level PV anomaly, maximum vector is 0.9 m s^{-1}; (c) at a height of 8 km, induced by the lower-level PV anomaly, maximum vector is 0.8 m s^{-1}; and (d) at a height of 2 km, induced by the lower-level PV anomaly, maximum vector is 9.5 m s^{-1}. Here, (0 km, 0 km) is the midlevel vortex center.

greater if heating and friction were included in the model.

4. Horizontal shear, diabatic heating, and friction

In this section we describe a calculation in which a vortex is initialized in a horizontal shear flow, including representations of diabatic heating and friction. The initial zonal flow is

$$\overline{U}_B = U_0 \cos\left(\frac{4\pi y}{L_y}\right),$$

where U_0 (=5 m s^{-1}) is constant and L_y = 8640 km. This flow is illustrated in Fig. 14a. The domain is 11 520 km in the x direction and 8640 km in the y direction with a horizontal resolution of 30 km. The vertical resolution is 2 km and the height of the domain is 14 km. The initial vorticity and tangential velocity profiles of the superposed vortex are similar to those used by Smith et al. (1990), but vary with height as shown in Fig. 14b and Fig. 14c. Note that the vortex is confined to the lower troposphere initially. Following Ooyama (1969), we assume that the latent heat released in deep convective clouds is proportional to the boundary layer convergence. Here, the flow includes a prescribed heating function that is related to the boundary layer conver-

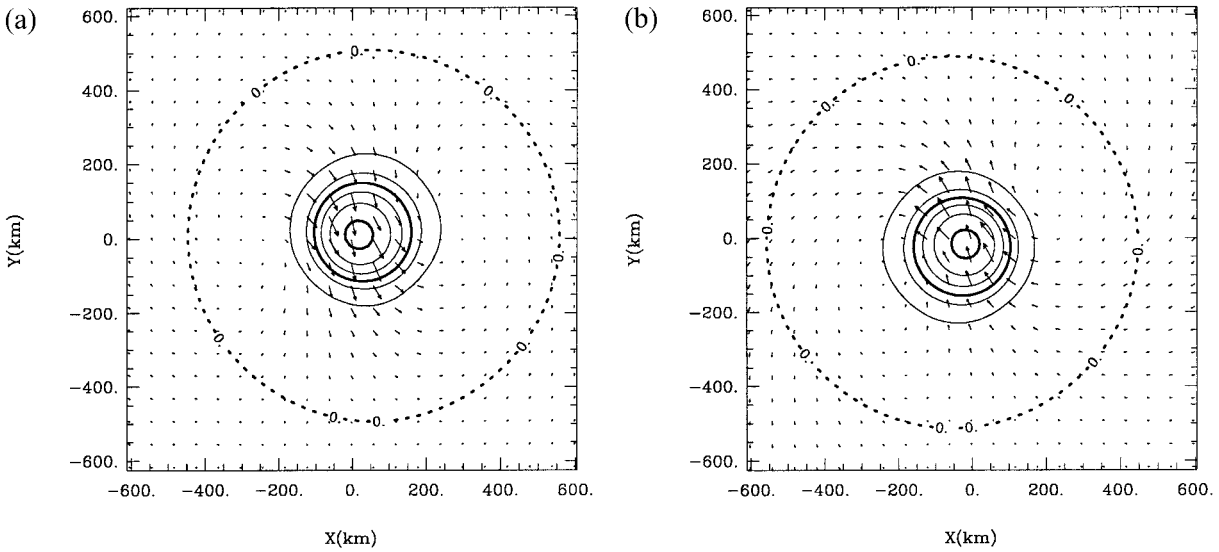

FIG. 13. Horizontal cross sections at 12 h and combined flows from the piecewise inversion. Arrows indicate the wavenumber-1 component of the horizontal wind. Contours of potential vorticity with contour interval 0.25×10^{-6} m^2 K/(s kg) (a) at a height of 2 km, induced by the upper- and lower-level PV anomalies, maximum vector is 8.6 m s^{-1}, and (b) at a height of 8 km, induced by the upper- and lower-level PV anomalies, maximum vector is 3.0 m s^{-1}. Here, (0 km, 0 km) is the midlevel vortex center.

gence. The heating function Q, which has a specified vertical profile, can be represented in the form that

$$Q(z) = \begin{cases} \chi(z) w_{\mathrm{BL}} & \text{if } w_{\mathrm{BL}} > 0 \\ 0 & \text{if } w_{\mathrm{BL}} \le 0, \end{cases} \tag{4.1}$$

where w_{BL} denotes the vertical velocity at the top of the boundary layer. In contrast to Ooyama (1969), who determines χ from energy considerations in terms of the enthalpy of moist air, it is sufficient for our purposes to define χ as 0.09 $\sin(\pi z/H)$ K m^{-1}, where H is 14 km and the maximum of heating occurs at 7 km.

The heating increases the PV below the heating maximum and reduces the PV above it. Therefore the cyclonic anomaly is strengthened below the heating maximum and an anticyclonic PV anomaly develops above the heating maximum. Consequently heating increases the cyclonic circulation at lower levels and leads to an anticyclonic circulation at upper levels. Figures 15a–c show vertical cross sections of the PV anomalies after 6, 12, and 24 h. We noted previously that the more negative the vorticity becomes, the greater the local Rossby number becomes and the greater is the inaccuracy of the AB theory. The negative relative vorticity in the upper-level anticyclone decreases the denominator of the squared local Rossby number R_L^2 and therefore R_L^2 increases at upper levels. In the present calculation, the vertical gradients in the tangential wind increased so much after 24 h that the baroclinic term in the denominator of R_L^2 became greater than the inertial stability term. Consequently, the symmetric PV became negative, which might be an indication that the vortex became inertially unstable so that the system was no longer in balance.

With heating included, the tangential velocity v' of the AB model became three orders of magnitude higher than that of the PE model. As the AB theory is derived for slowly evolving vortices, the acceleration term is assumed to remain small. Inclusion of the heating, however, implies the existence of fast inertial–gravity waves, which involve large accelerations. To keep Eq. (3.7) of SM consistent with the tendency equation (3.10) of SM, it is necessary to drop the first, second, and fourth terms of the right-hand side of $D_v w'/Dt$, where w' is given by (3.9) of SM. Then SM's (3.7) becomes

$$v' = \frac{1}{\bar{\xi}} \frac{\partial \phi'}{\partial r} - \frac{1}{\bar{\eta}\bar{\xi}} \frac{1}{r} \frac{D_v(\partial \phi'/\partial \lambda)}{Dt} - \frac{\partial \bar{v}/\partial z}{\bar{\eta}\bar{\xi}} \frac{D_v}{Dt}\left(\frac{\bar{\xi}}{\partial z} \frac{\partial \bar{v}}{\partial r} \frac{1}{r} \frac{\partial \phi'}{\partial \lambda} \right), \tag{4.2}$$

and the acceleration terms in the tangential velocity equation and hence in the PV equation are suppressed.

After 12 h the vortex has moved 200 km to the east and very slightly to the south. The translation velocity components are $c_x = 4.7$ m s^{-1}, $c_y = 0.2$ m s^{-1}, and the acceleration $\dot{\mathbf{c}}$ is on the order of 10^{-6} m s^{-2}. The horizontal shear flow contributes to the symmetric part of the vortex. The magnitude and indeed the sign of this contribution depends on the location of the vortex center, as can be seen by referring to Fig. 14a. When the center of the vortex is south of the background flow maximum (i.e., south of the east–west line labeled 0 km in Fig. 14a), an azimuthal average of the background flow contributes a negative tangential velocity and leads in this case to a negative relative vorticity. If the negative relative vorticity exceeds a certain value, R_L^2 becomes negative and no AB solution can be found. In

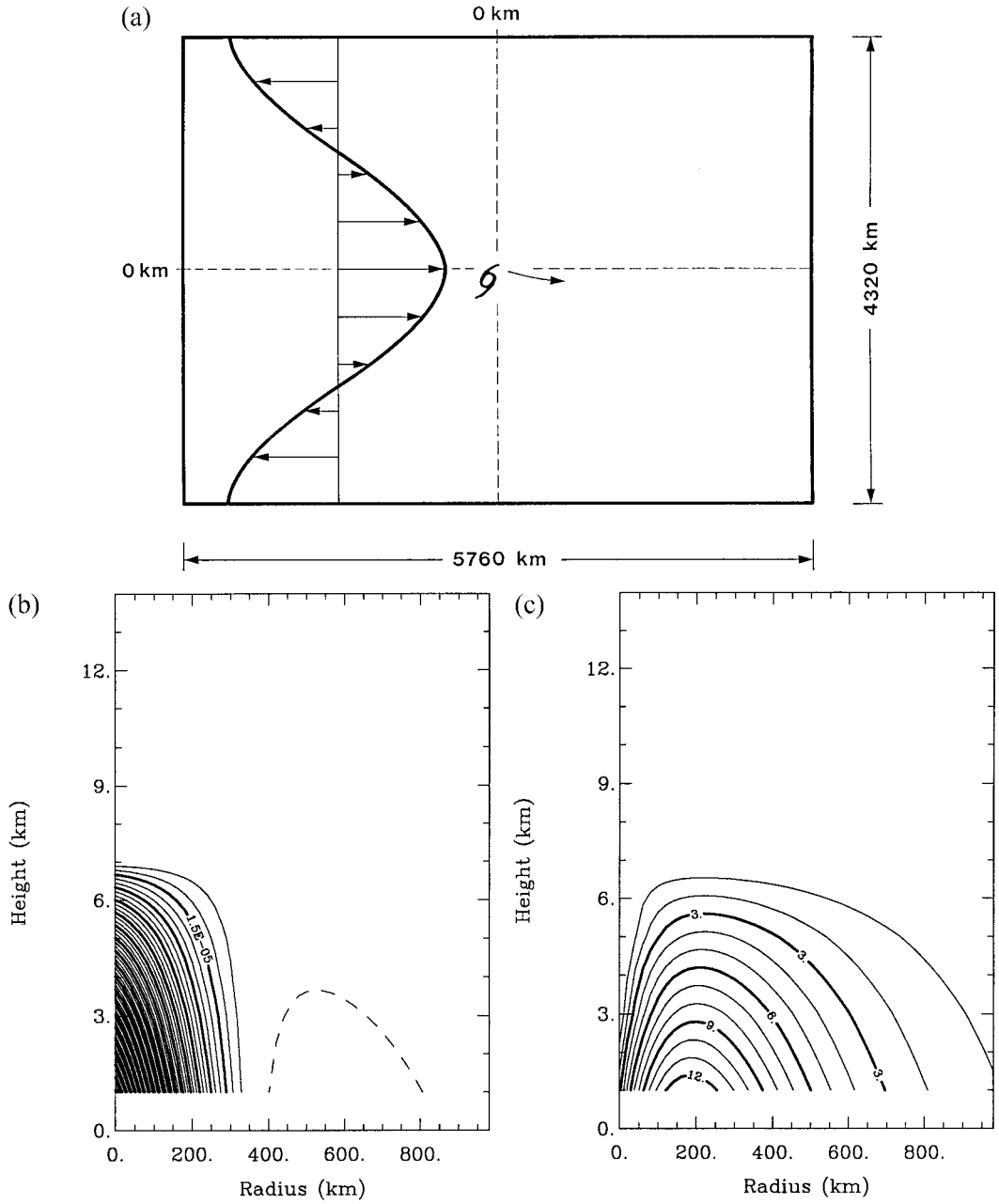

FIG. 14. Initial conditions for calculations with heating. (a) Horizontal shear flow in which the vortex is embedded. The vortex moves to the east and slightly to the south. Only the central part of the domain is shown. (b) Radial–height cross section of the relative vorticity (contour interval 0.5×10^{-5} s^{-1}). (c) Radial-height cross section of the tangential velocity in m s^{-1} of the initial vortex in section 4.

order to obtain a positive R_L^2 initially, we subtracted the background flow contribution from the symmetric part of the vortex in the AB calculation. Similar problems would arise in obtaining a solution in any balanced formulation when the PV becomes negative. The presence of negative PV usually necessitates an ad hoc adjustment of the PV to be positive (see, e.g., Davis and Emanuel 1991) and is a particularly severe test of the theory. The absence of the contribution from the background flow in the AB calculation increases the difference between it and the corresponding velocity components in the PE calculation.

Results are presented at 6 and 12 h. An upper-level anticyclone is induced by the heating and increases the local Rossby number squared R_L^2, isopleths of which are shown in Fig. 16. The maximum of R_L^2 is about 0.24 after 6 h, and increases to 0.44 after 12 h, becoming negative at 24 h. In the first 12 h, a vortex had not developed at upper levels, and $v' > \overline{v}$ above a height of about 5 km. Thus the asymmetric wind is not a small

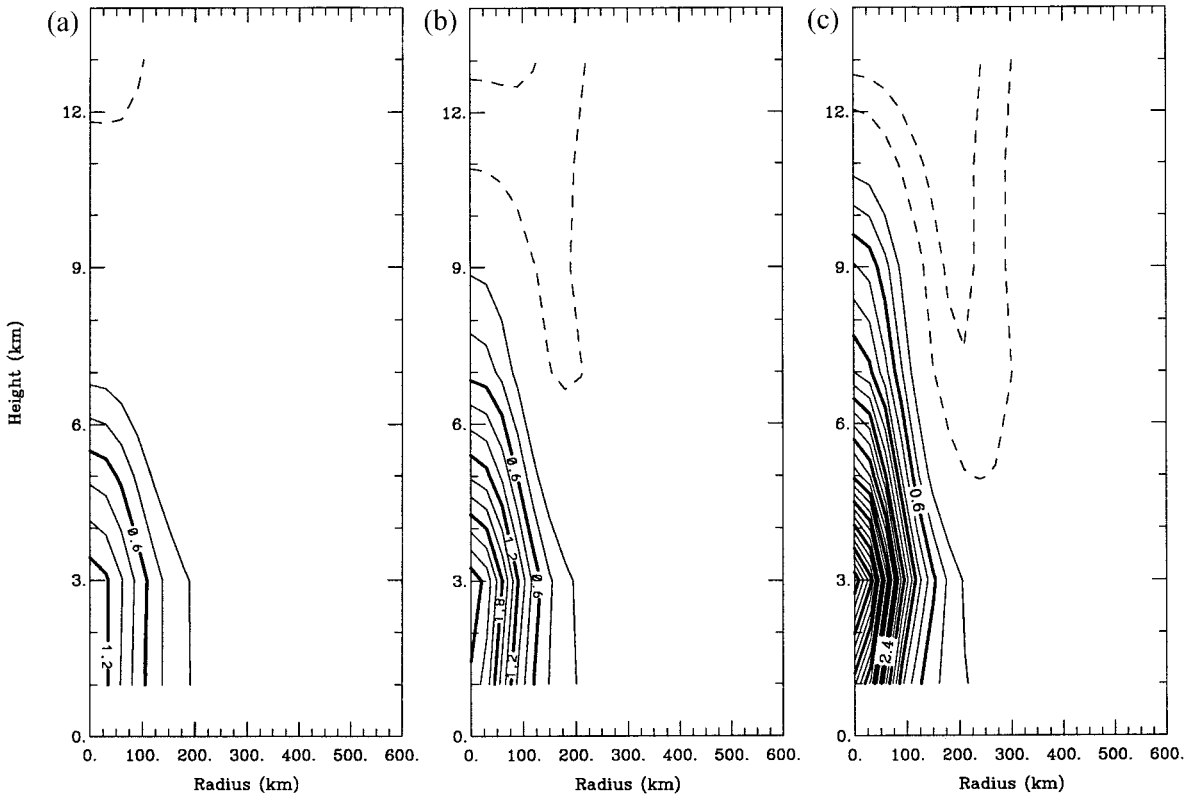

FIG. 15. Radial–height cross sections of the PV anomalies. Contour interval is 0.2×10^{-6} m^2 K/(s kg) (a) after 6 h, (b) after 12 h, and (c) after 24 h.

linear perturbation on the symmetric vortex in this region and it is necessary to use the standard Rossby number Ro as a measure for the validity and accuracy of the approximation as in quasigeostrophy. The standard Rossby number Ro is calculated with the total tangential velocity v (Ro $= v/fr$). At 6 h $v' = 4.9$ m s^{-1} at a radius of 150 km and at 12 h $v' = 5.1$ m s^{-1} at a radius of 120 km, giving Ro $= 0.66$ after 6 h and Ro $= 0.85$ after 12 h. Since Ro is not small outside the vortex, we can expect the AB theory to be inaccurate at the upper levels. As in section 3, a comparison is made between the wavenumber-1 distributions of the tangential and radial wind fields of the AB and PE models. It can be assumed that even here, where heating is included, the results of the PE and AB models should be similar as long as R_L^2 in and Ro outside the vortex core region are small.

The results show very clearly that the accuracy of the AB solution decreases as R_L^2 increases. Only with a reasonably small R_L^2 (<1) or Ro < 1 in the quasigeostrophic regime at large distances from the vortex is it possible to obtain reasonably accurate results with the theory. For Ro and $R_L^2 \sim \frac{1}{3}$, the accuracy of an AB solution lies between $\pm(\frac{1}{3})$. Figures 17–19 show the wavenumber-1 distributions of the tangential and radial velocity components after 6 and 12 h at heights of 2 and 6 km. The radial velocity shows a wavenumber-1 pattern with extrema oriented east–west. The tangential velocity shows a north–south orientation of the extrema. In both velocity components there is a change in sign with increasing radius that results from the contribution of the wavenumber-1 component of the background flow. In fact, the contribution from the background flow dominates the wavenumber-1 velocity fields. The orientation of the wavenumber-1 patterns are the same for the PE and AB calculations. After 6 h the maxima of the amplitudes of u'_{PE} is 4.7 m s^{-1} (Fig. 17a) and of u'_{AB} is 7.4 m s^{-1} (Fig. 17b), $v'_{PE} = 4.9$ m s^{-1} (Fig. 17c), and $v'_{AB} = 5.7$ m s^{-1} (Fig. 17d) at a height of 2 km. At a height of 6 km, the PE calculations have a similar amplitude as at a height of 2 km, whereas the AB calculations show significant differences in the amplitude. At a height of 6 km u'_{PE} has a maximum of 4.8 m s^{-1} (Fig. 18a), and $u'_{AB} = 10.9$ m s^{-1} (Fig. 18b), $v'_{PE} = 4.9$ m s^{-1}, and $v'_{AB} = 8.0$ m s^{-1} (Figs. 18c and 18d). After 12 h the results of the PE calculations stay the same, since there is no significant change in the background flow, and we show only the results from the AB calculations. At the heights of 2 and 6 km, the orientation of the velocity fields stays the same. At a height of 2 km there is not a large difference in the amplitudes of u'_{AB} and v'_{AB} compared with the values after 6 h, and $u'_{AB} = 7.5$ m s^{-1} and $v'_{AB} = 5.6$ m s^{-1} (Figs. 19a and 19b). At a

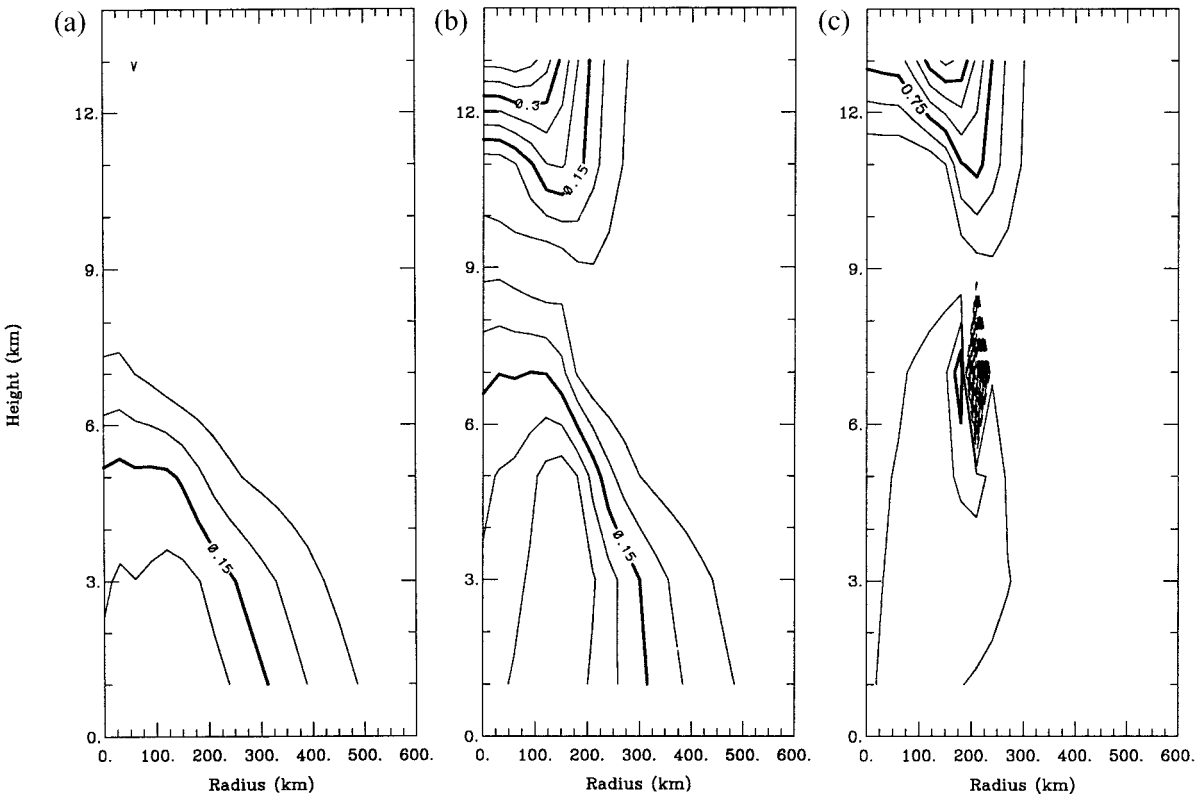

FIG. 16. Radial–height cross sections of the squared local Rossby number (a) after 6 h, (b) after 12 h, and (c) after 24 h. Contour interval is 0.05 for (a) and (b), and 0.25 for (c).

height of 6 km $u'_{AB} = 14.1$ m s^{-1} and $v'_{AB} = 8.4$ m s^{-1} (Figs. 19c and 19d).

Compared with the results after 6 h, the greater error after 12 h in the calculation from the AB theory is caused by the higher inaccuracy in the approximations, which is in accord with the higher local Rossby number of Fig. 16b. After 24 h the flow is not in balance, as indicated by the negative local Rossby number in Fig. 16c. In a case where we tried to initialize the vortex with a vertical shear flow, we obtained an unbalanced state after the first few hours. The solution in the AB theory diverged after the first iteration and no solution could be found. If heating is included in the calculation, the PV becomes negative after a certain period of time. Just as in the nonlinear balance equations (Davis and Emanuel 1991) the AB formulation requires the PV to be positive. In the case of the AB theory, the condition that the PV of the symmetric vortex is positive is identical to the condition that the discriminant of the operator in the geopotential tendency equation (2.1) is positive. If the PV of the symmetric vortex is negative, then the system is not elliptic and there is no balanced solution. Of course the stronger condition for the accuracy of the AB theory that the local Rossby number is small (but positive), when satisfied, guarantees that the symmetric PV is positive and that a balanced solution exists.

5. Summary and discussion

This paper has presented results from PV inversion using a three-dimensional diagnostic balance model for tropical cyclones. The model is based upon the asymmetric balance (AB) theory derived by Shapiro and Montgomery (1993). The main advantage of the AB theory is its ability to represent the large divergence that occurs in a hurricane. The standard balance equations neglect divergence relative to the vorticity. The AB theory takes advantage of the weakness of the asymmetries in a hurricane relative to the much stronger basic state. As the wavenumber 1 dominates the total asymmetry in the vortex core region it is sufficient to apply the AB theory for wavenumber 1 only. In the quasigeostrophic regime at large distance from the vortex, the asymmetries with wavenumbers greater than 1 must also be included.

The diagnostic application of the AB theory was explained. We showed how the two fundamental AB equations have to be manipulated and how the geopotential, its local time tendency, and its second-order time tendency can then be evaluated at a given time. We found that the nonlinear terms, which—following Shapiro and Montgomery—have to be added in the quasigeostrophic regime, became dominant near the vortex center, which contradicts the fact that the asymmetries are assumed

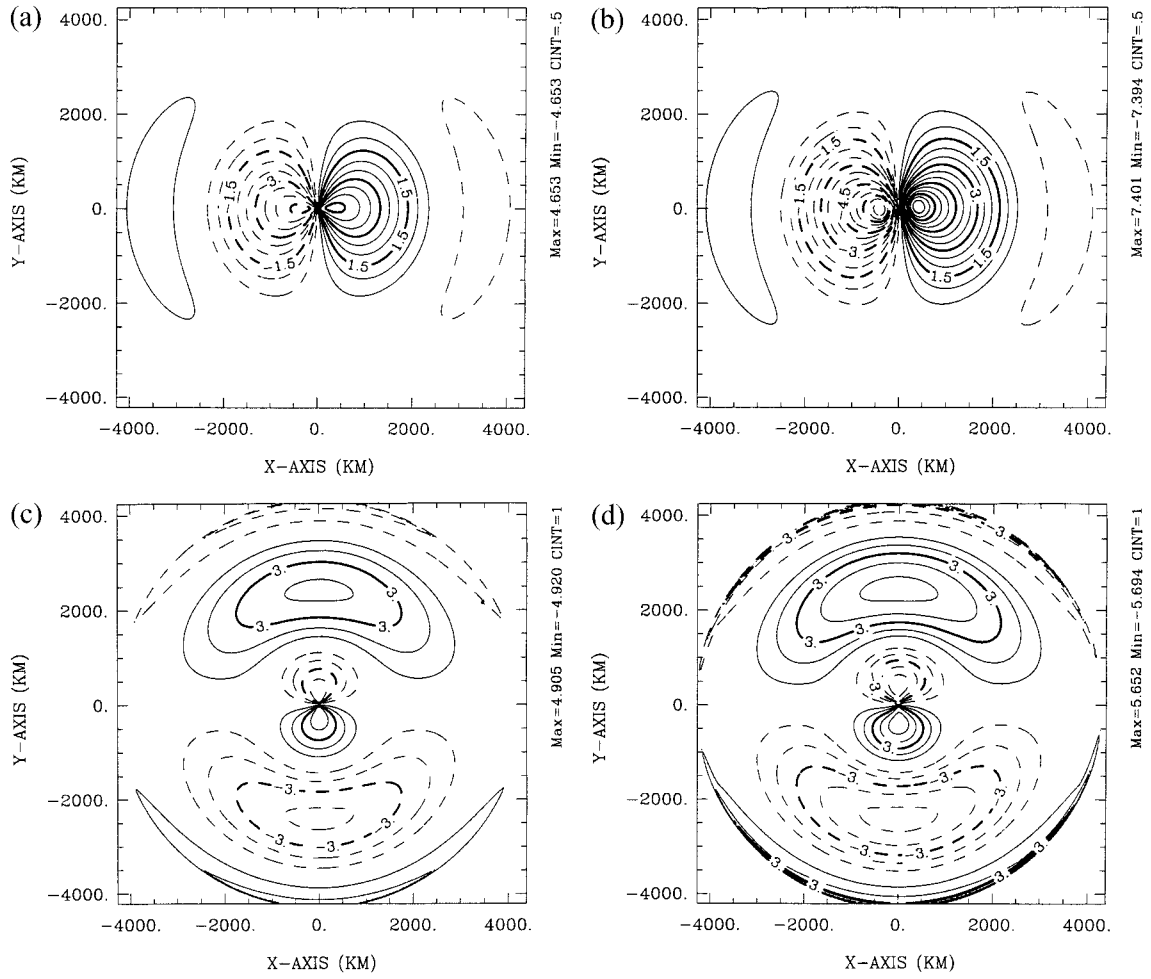

FIG. 17. Horizontal cross sections of the wavenumber-1 component after 6 h at a height of 2 km: (a) the radial velocity u calculated with the PE model, (b) the radial velocity u calculated with the AB model, (c) tangential velocity v calculated with the PE model, and (d) tangential velocity v calculated with the AB model. Contour interval is 0.5 m s^{-1} for (a) and (b) and 1.0 m s^{-1} for (c) and (d). Here, (0 km, 0 km) is the vortex center; this corresponds to (−920 km, −20 km) in x–y space.

to be weak in the vortex center. We were able to find a method to include the nonlinear terms only in the vortex far field where they are important. We described how the friction could be incorporated in the AB theory by including terms that involve bulk drag coefficients in the momentum equations, the geopotential tendency equation, and the PV equation.

The total PV was inverted using an iterative technique to solve the geopotential tendency equation and the PV equation simultaneously. A fundamental aspect of the AB theory is that it is formulated in a coordinate system that translates with the vortex. Therefore, in a baroclinic experiment where the translation speed is different at each level it is important to find the level that represents the vortex translation speed best. This is necessary to maintain accuracy of the AB theory.

A PE model was used to provide the datasets for the PV inversion. The first model calculation described an initially barotropic vortex in a vertical shear. In response to the vertical shear, the vortex tilts and a cyclonic rotation of the upper- and lower-level vortices about the middle-level vortex center was observed. This leads to a wavenumber-1 distribution of the PV and wind fields. The AB theory was able to reproduce the height and wind fields obtained from the PE model. The results served as a test of the new AB theory. The fundamental approximation in the AB theory is the assumption that the square of the advective rate-of-change is much smaller than the inertial stability of the vortex. The ratio of the orbital frequency squared to the inertial stability is defined by the *local* Rossby number squared, R_L^2, which is assumed to be $\ll 1$. The size of R_L^2 depends also on the vortex relative vorticity distribution, as the absolute vorticity occurs in the denominator of R_L^2. When the absolute vorticity becomes small, R_L^2 becomes large and the AB theory becomes inaccurate. The AB model velocity fields agreed very well in orientation and amplitude with those of the PE model. At lower

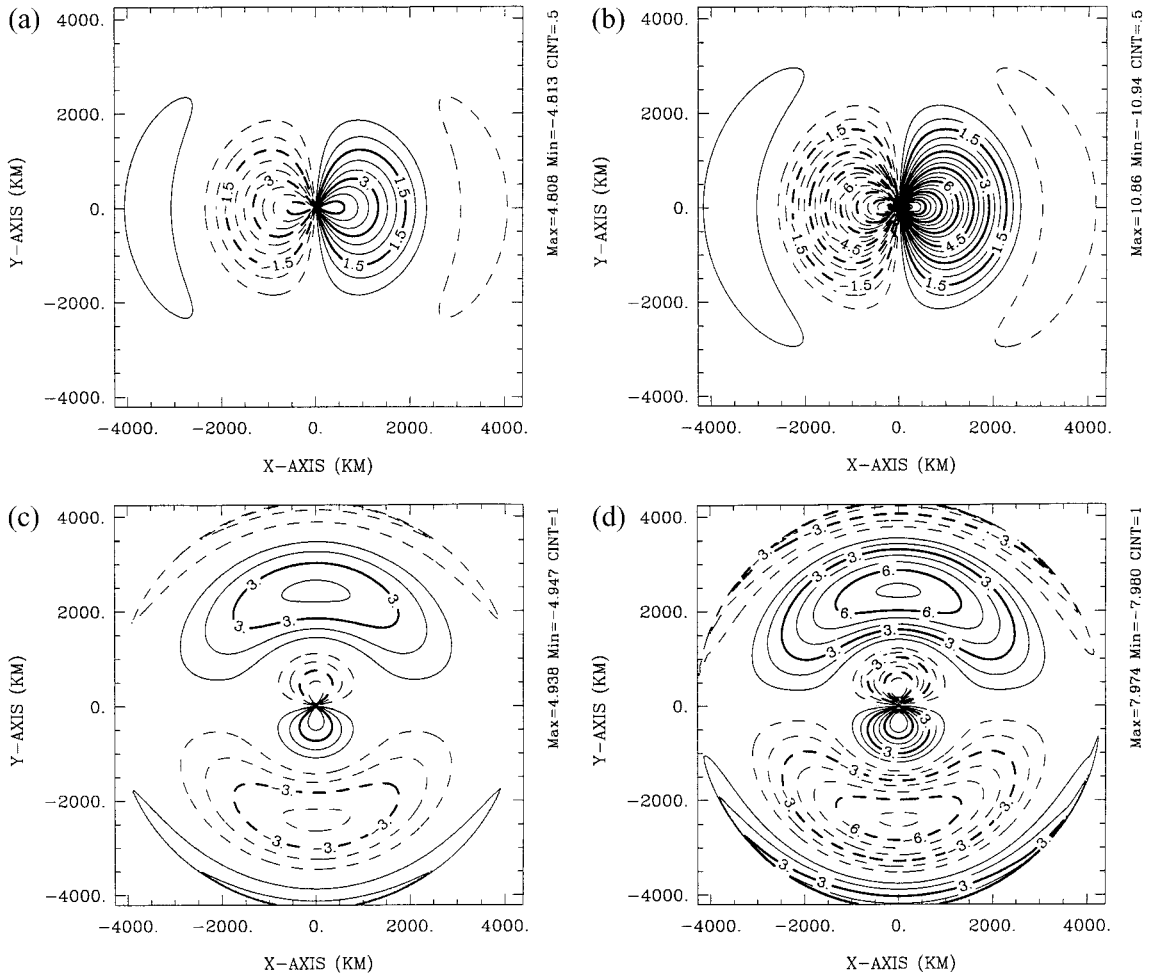

FIG. 18. As in Fig. 17 but at a height of 6 km.

levels of the domain, the relative error between the amplitudes of the AB and PE calculations was comparable in size to R_L^2. This confirms that the inaccuracy of the AB theory increases with R_L^2.

The role played by individual portions of the PV field was investigated by performing a piecewise PV inversion. Presenting the results of the velocity fields in the moving coordinate system and using the piecewise inversion made it possible to isolate the influence of the upper-level PV anomaly on the lower-level part of the vortex and the influence of the lower-level PV anomaly on the upper-level part of the vortex. The issue regarding which level to use for defining the center of the vortex for the piecewise inversion is not fundamental to the AB theory and is, in fact, present whenever a symmetric vortex is used to define the basic state. The greater the vortex tilt, the more important this issue could be. Möller (1995, section 7.3) discusses the sensitivity of the result to the choice of level more completely. Convective coupling in a more realistic model calculation or an observed hurricane, however, would be expected to reduce the tilt and to minimize this sensitivity.

We calculated the wind fields for the same experiment using the quasigeostrophic approximation. As expected this approximation was not able to represent the vortex core region. The orientation of the velocity fields were similar, but the amplitudes were about one order of magnitude higher than in the PE calculation.

Diabatic heating and friction were included in a calculation where the vortex was embedded in a horizontal shear flow. The prescribed heating was related to the boundary layer convergence. The heating creates positive PV at low levels, thereby increasing the cyclonic circulation. At upper levels the heating creates a negative PV anomaly and an anticyclonic circulation develops. In these experiments divergence above the boundary layer was not large.

We found that the inclusion of heating resulted in values of the tangential velocity three orders of magnitude larger than the tangential velocity of the PE model. However, when the acceleration terms were omitted in the tangential velocity equation, we obtained reasonable tangential velocity fields at lower levels. Neglect of the acceleration terms is consistent with the tendency

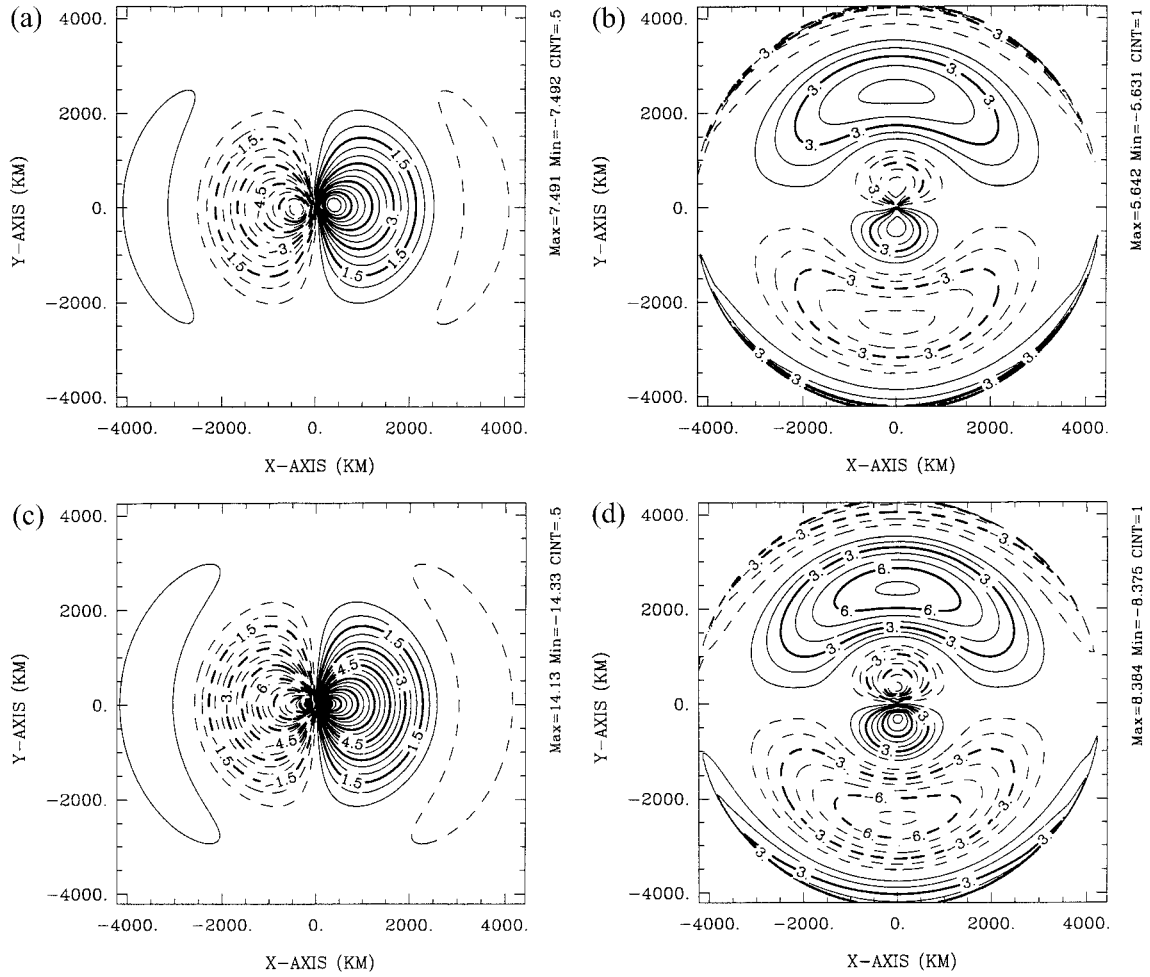

FIG. 19. Horizontal cross sections of the wavenumber-1 component of the radial velocity u and tangential velocity v after 12 h calculated with the AB model. At a height of 2 km (a) radial velocity and (b) tangential velocity. At a height of 6 km (c) radial velocity and (d) tangential velocity. Contour interval is 0.5 m s^{-1} for (a) and (c) and 1.0 m s^{-1} for (b) and (d). (0 km, 0 km) is the vortex center; this corresponds to (−820 km, −20 km) in x–y space.

equation. The heating produced strong vertical gradients in the tangential wind so that the PV of the symmetric vortex became negative after 24 h. A negative PV of the symmetric vortex implies a negative squared local Rossby number. As in the nonlinear balance equations, the AB formulation requires the PV to be positive in order to be able to find a solution.

It was noted previously that the local Rossby number becomes greater the more negative the relative vorticity becomes. This leads to greater inaccuracy in the AB theory. In the calculation with diabatic heating, the anticyclonic upper-level vortex became stronger with time and therefore the negative relative vorticity became greater, increasing R_L^2. The maximum of R_L^2 was about 0.24 after 6 h and 0.44 after 12 h. At upper levels a vortex had not developed after 12 h and the tangential perturbation velocity v' was greater than the symmetric velocity $\overline{v}$, violating a central approximation of the AB theory. Consequently, we could not apply the squared local Rossby number as a measure for the validity and accuracy since the AB theory demands that $\overline{v} > v'$. In this case the standard Rossby number Ro was the appropriate measure of the validity and accuracy as in the quasigeostrophic approximation: Ro was 0.66 after 6 h and 0.85 after 12 h. A comparison was made of the velocity components of the AB and PE model at 2 km and 6 km. The orientation of the wavenumber-1 distributions of the radial and tangential wind components were in good agreement. The amplitudes of the winds were similar for both models at a height of 2 km but differed at a height of 6 km. The relative error in the amplitudes were for the data at the height of 2 km similar to the magnitude of R_L^2 and for the data at the height of 6 km similar to the magnitude of Ro.

This study is the first to demonstrate the viability of the AB theory in a three-dimensional context. However, we have found problems in applying the theory when the effects of heating and friction are included. The

accuracy of the theory is characterized by a squared local Rossby number R_L^2. If the standard Rossby number Ro is large in the inner vortex region, the theory gives accurate results as long as the squared *local* Rossby number is small. In particular, negative PV makes it impossible to find a solution of the balance system. It should be noted, that no balance theory has a solution when the PV is negative. This negative PV is associated with the anticyclone in the upper level of the domain. Whether or not the PV is negative depends on the strength of the anticyclone. Our results show that the AB theory is not able to characterize the motion in the outflow layer in the case we studied. However, because of our crude representation of heating we cannot be sure that the strength of the anticyclone in our numerical calculation is realistic for a hurricane. In particular, our use of a fixed heating profile means that we are unable to represent the mature phase of a tropical cyclone since changes in the stability in the core of the cyclone do not alter the strength of the diabatic heating. If the anticyclone were weaker, it is possible that the PV would not have been negative, in which case we may have been able to characterize the motion in the outflow layer. Figure 1 shows that for Hurricane Gloria the asymmetric divergence had a comparable size to the asymmetric vorticity. SM showed that the squared local Rossby number (R_L^2) is positive and less than 0.5 everywhere in Hurricane Gloria. This suggests that a balanced AB solution should be possible for the Gloria data, although the solution might be inaccurate in certain regions. Hurricane Gloria is one of the best observed hurricanes, but the lack of data in the outflow layer makes the analysis in this region questionable. Future work is necessary to apply the AB theory to a case where the divergence is large and to compare the results with those of the standard balanced models. The AB theory gives an alternative to the standard balance equations and can be applied to the inner core regions of tropical cyclones. Indeed, it is the only theory that is *formally* valid in regimes of large Rossby number and moderate Froude number.

Acknowledgments. The work presented in this paper would not have been possible without the support and encouragement of Roger Smith, to whom we express our sincere thanks. We are also very grateful to Michael Montgomery and Lloyd Shapiro for their most helpful comments. We especially appreciate Lloyd Shapiro's advice on piecewise inversion. We gratefully acknowledge James Franklin for providing Fig. 1. The comments of Dan Keyser, John Molinari, and an anonymous reviewer on an earlier version helped us to improve this manuscript. This work was supported by the German Research Council (DFG) and the U.S. Office of Naval Research through Grant N00014-95-1-0394.

REFERENCES

Anthes, R. A., 1982: *Tropical Cyclones—Their Evolution, Structure and Effects. Meteor. Monogr.*, No. 41, Amer. Meteor. Soc., 208 pp.

Charney, J. G., 1962: Integration of the primitive and balance equations. *Proc. Int. Symp. on Numerical Weather Prediction,* Tokyo, Japan, Meteor. Soc. Japan, 131–152.

Davis, C. A., 1992: Piecewise potential vorticity inversion. *J. Atmos. Sci.,* **49,** 1397–1411.

——, and K. A. Emanuel, 1991: Potential vorticity diagnostics of cyclogenesis. *Mon. Wea. Rev.,* **119,** 1929–1953.

Ertel, H., 1942: Ein neuer hydrodynamischer Wirbelsatz. *Meteor. Z.,* **59,** 271–281.

Fiorino, M., and R. L. Elsberry, 1989: Some aspects of vortex structure related to tropical cyclone motion. *J. Atmos. Sci.,* **46,** 975–990.

Franklin, J. L., S. J. Lord, S. E. Feuer, and F. D. Marks Jr., 1993: The kinematic structure of Hurricane Gloria (1985) determined from nested analyses of dropwindsonde and Doppler radar data. *Mon. Wea. Rev.,* **121,** 2433–2451.

Hakim, G. J., D. Keyser, and L. F. Bosart, 1996: The Ohio Valley wave-merger cyclogenesis event of 25–26 January 1978. Part II: Diagnosis using quasigeostrophic potential vorticity inversion. *Mon. Wea. Rev.,* **124,** 2176–2205.

Hoskins, B. J., 1975: The geostrophic momentum approximation and the semi-geostrophic equations. *J. Atmos. Sci.,* **32,** 233–242.

——, and F. P. Bretherton, 1972: Atmospheric frontogenesis models: Mathematical formulation and solution. *J. Atmos. Sci.,* **29,** 11–37.

——, M. E. McIntyre, and A. W. Robertson, 1985: On the use and significance of isentropic potential vorticity maps. *Quart. J. Roy. Meteor. Soc.,* **111,** 877–946.

Houze, R. A., Jr., 1993: *Cloud Dynamics.* Academic Press, 573 pp.

Jones, S. C., 1995: The evolution of vortices in a vertical shear. Part I: Initially barotropic vortices. *Quart. J. Roy. Meteor. Soc.,* **121,** 821–851.

——, and A. J. Thorpe, 1992: The three-dimensional nature of ''symmetric'' instability. *Quart. J. Roy. Meteor. Soc.,* **118,** 227–258.

Keyser, D., B. D. Schmidt, and D. G. Duffy, 1992: Quasigeostrophic diagnosis of three-dimensional ageostrophic circulations in an idealized baroclinic disturbance. *Mon. Wea. Rev.,* **120,** 698–730.

McWilliams, J. C., 1985: A uniformly valid model spanning the regimes of geostrophic and isotropic, stratified turbulence: Balanced turbulence. *J. Atmos. Sci.,* **42,** 1773–1774.

——, and P. R. Gent, 1980: Intermediate models of planetary circulations in the atmosphere and ocean. *J. Atmos. Sci.,* **37,** 1657–1678.

——, ——, and N. J. Norton, 1986: The evolution of balanced, low-mode vortices on the beta-plane. *J. Phys. Oceonogr.,* **16,** 838–855.

Miller, B. I., 1964: A study of the filling of Hurricane Donna (1960) over land. *Mon. Wea. Rev.,* **92,** 389–406.

Molinari, J., S. Skubis, and D. Vollaro, 1995: External influences on hurricane intensity. Part III: Potential vorticity structure. *J. Atmos. Sci.,* **52,** 3593–3606.

Möller, J. D., 1995: Tropical cyclones: A potential vorticity perspective. Ph.D. thesis, University of Munich, 110 pp. [Available from Dr. J. D. Möller, Dept. of Atmospheric Science, Colorado State University, Fort Collins, CO 80523-1371.]

Montgomery, M. T., and B. F. Farrell, 1992: Polar low dynamics. *J. Atmos. Sci.,* **49,** 2484–2505.

Ooyama, K. V., 1969: Numerical simulation of the life cycle of tropical cyclones. *J. Atmos. Sci.,* **26,** 3–40.

Raymond, D. J., 1992: Nonlinear balance and potential-vorticity thinking at large Rossby number. *Quart. J. Roy. Meteor. Soc.,* **118,** 987–1015.

Robinson, W. A., 1988: Analysis of LIMS data by potential vorticity inversion. *J. Atmos. Sci.,* **45,** 2319–2342.

——, 1989: On the structure of potential vorticity in baroclinic instability. *Tellus,* **41A,** 275–284.
Roll, H. U., 1965: *Physics of the Marine Atmosphere.* Academic Press, 426 pp.
Rotunno, R., and J.-W. Bao, 1996: A case study of cyclogenesis using a model hierarchy. *Mon. Wea. Rev.,* **124,** 1051–1066.
Schubert, W. H., P. E. Ciesielski, D. E. Stevens, and H.-C. Kuo, 1991: Potential vorticity modeling of the ITCZ and the Hadley circulation. *J. Atmos. Sci.,* **48,** 1493–1509.
Shapiro, L. J., and K. V. Ooyama, 1990: Barotropic vortex evolution on a beta-plane. *J. Atmos. Sci.,* **47,** 170–187.
——, and M. T. Montgomery, 1993: A three-dimensional balance theory for rapidly rotating vortices. *J. Atmos. Sci.,* **50,** 3322–3335.
——, and J. L. Franklin, 1995: Potential vorticity in Hurricane Gloria. *Mon. Wea. Rev.,* **123,** 1465–1475.
Smith, R. K., 1968: The surface boundary layer of a hurricane. *Tellus,* **20,** 473–484.
——, W. Ulrich, and G. Dietachmayer, 1990: A numerical study of tropical cyclone motion using a barotropic model. Part I: The role of vortex asymmetries. *Quart. J. Roy. Meteor. Soc.,* **116,** 337–362.
Thorpe, A. J., and C. H. Bishop, 1995: Potential vorticity and the electrostatics analogy: Ertel-Rossby formulation. *Quart. J. Roy. Meteor. Soc.,* **121,** 1477–1495.
Willoughby, H. E., 1979: Excitation of spiral bands in hurricanes by interaction between the symmetric mean vortex and a shearing environmental steering current. *J. Atmos. Sci.,* **36,** 1226–1235.
——, 1988: Linear motion of a shallow-water, barotropic vortex. *J. Atmos. Sci.,* **45,** 1906–1928.
Wu, C.-C., and K. A. Emanuel, 1995a: Potential vorticity diagnostics of hurricane movement. Part I: A case study of Hurricane Bob (1991). *Mon. Wea. Rev.,* **123,** 69–92.
——, and ——, 1995b: Potential vorticity diagnostics of hurricane movement. Part II: Tropical Storm Ana (1991) and Hurricane Andrew (1992). *Mon. Wea. Rev.,* **123,** 93–109.